Integration of ARGO trajectories in the Mediterranean Forecasting System and impact on the regional analysis of the Western Mediterranean circulation

by

V. Taillandier[1], S. Dobricic[2], P. Testor[3], N. Pinardi[4], A. Griffa[5, 6], L. Mortier[3], G.P. Gasparini[5]

[1] LOV-CNRS, Villefranche-sur-Mer, France

[2] CMCC, Bologna, Italy

[3] LOCEAN-IPSL, Paris, France

[4] INGV, Bologna, Italy

[5] CNR-ISMAR, La Spezia, Italy

[6] RSMAS, University of Miami, Florida, USA

submitted to

Journal of Geophysical Research

third revised version

September 15, 2009

corresponding author:

Vincent Taillandier, LOV-CNRS, Quai de la Darse, 06230 Villefranche-sur-Mer, France

tel: +33 4 93 76 37 36; e-mail: taillandier@obs-vlfr.fr

Abstract

The impact of ARGO float trajectory assimilation on the quality of ocean analyses is studied by means of an operational oceanographic model implemented in the Mediterranean Sea and a 3D-var assimilation scheme. For the first time, both ARGO trajectories and vertical profiles of temperature and salinity (TS) together with satellite altimeter data of sea level anomaly (SLA) are assimilated to produce analyses for short term forecasts. The study period covers three months during winter 2005 when four ARGO trajectories were present in the northwestern Mediterranean Sea. The scheme is first assessed computing the misfits between observations and model forecast and analysis. The misfit statistics appear improved for float trajectories, while they are not degraded for the other assimilated variables (TS profiles and SLA). This indicates that the trajectory integration is consistent with the other components of the assimilation system, and provides new information on horizontal pressure gradients. Comparisons between analyses obtained with and without trajectory assimilation suggest that trajectory assimilation can impact on the description of boundary currents and their instabilities, as well as mesoscale activity at regional scales. Changes are depicted by intermediate water mass redistributions, mesoscale eddy relocations and net transport modulations. These impacts are detailed and assessed considering historical and simultaneous in-situ datasets. The results motivate the integration of ARGO trajectories in the operational Mediterranean Forecasting System.

1. Introduction

In a regional sea like the Mediterranean, the basin scale circulation is strongly influenced by mesoscale features. They are triggered by vertical mixing or baroclinic instability (Crépon et al., 1982), generating eddies (up to ~100km of diameter) whose lifetime can span several months or even years (Puillat et al., 2002; Taupier-Letage et al., 2003). These mesoscale features significantly influence momentum and thermohaline fluxes. The large eddies can strongly perturb and in some cases even block the large scale circulation (Bouzinac et al., 1999; Testor et al., 2005a). The smaller eddies (~10-20km of diameter) contribute significantly to the formation and spreading of dense waters by acting on dispersion and on lateral mixing (Madec et al., 1996; Testor and Gascard, 2006; Demirov and Pinardi, 2007). At the shelf interface, they may strongly influence the renewal of coastal waters through the regulation of offshore exchanges (e.g., Mariano et al., 2003). For these reasons, observations and models that resolve the mesoscale variability need to be considered together, in order to provide best estimates and forecasts of the Mediterranean circulation.

The Mediterranean Forecasting System (hereafter MFS) has been developing the observational and modeling bases for the estimation of the circulation at the basin scale with mesoscale resolution (Pinardi et al., 2003). Observing systems have been designed and implemented for routine and automated monitoring of the oceans, even at the mesoscale in the main Mediterranean sub-basins. The monitoring is realized in first instance by a constellation of three satellite altimeters (Jason, ERS, Topex/Poseidon; Le Traon et al., 2003). Satellite radiometers are also an integral part of the remote sensing component (Buongiorno Nardelli et al., 2003; Marullo et al., 2007). In-situ observing efforts have been concentrated on Ship of Opportunity Programs (Manzella et al., 2007), surface drifters and autonomous ARGO float profilers (Poulain et al., 2007), mooring networks (Nittis et al., 2007), and glider sections (Dobricic et al., in revision). In parallel, circulation models have been upgraded in order to fully resolve the mesoscale dynamics (Béranger et al., 2005; Tonani et al., 2008). Assimilation techniques have also been upgraded in

order to provide multivariate analysis of the ocean circulation (Dobricic et al., 2005, 2007) permitting enhanced dynamical constraints (Dobricic and Pinardi, 2008).

Thanks to these developments, the MFS nowadays assimilates satellite altimeters along track data and vertical hydrological profiles of temperature (T) from XBTs and temperature and salinity (S) from ARGO float profilers. Profilers have been deployed in the frame of the MedArgo program (Poulain et al., 2007; http://poseidon.ogs.trieste.it/sire/medargo). Their cycling characteristics have been specifically tailored for the Mediterranean Sea (see Figure 1 in Poulain et al., 2007): a cycle period of approximately five days has been chosen to resolve the expected mesoscale variability, and a parking depth of 350 m has been fixed to track the core of the Levantine Intermediate Water (LIW), which is one of the main Mediterranean water masses.

At present, ARGO float trajectories are not routinely integrated in the MFS, even though they contain direct information on ocean currents in the open sea as well as near the shelf. Assimilating trajectory data is challenging for a number of reasons (Kamachi and O'Brien, 1995; Ishikawa et al., 1996; Ozgokmen et al., 2000; Ide et al., 2002), which motivated suitable methodologies developed only in the last few years (Molcard et al., 2003, 2005; Kuznestov et al. 2003; Taillandier et al., 2006a, Nodet, 2006). For example in Taillandier et al. (2006a), the issue of the non-linear relationship between float position data, that describe the subsurface drift between two profiles and the ocean current estimates, has been tackled using a variational and Lagrangian formalism. An application of this method for the assimilation of ARGO-like trajectories has been reported in Taillandier and Griffa (2006). In this study, specific sampling issues related to ARGO profilers have been investigated using the OSSE (Observing System Simulation Experiment) approach with virtual floats. The fact that ocean currents are measured rather sparsely with a trajectory sampling of some days and rather noisily due to the non-measurable shear drifts experienced during the profiling sequences has been quantified in terms of potential efficiency for their assimilation.

Thanks to these preliminary investigations, a first test of assimilation of in-situ ARGO trajectories in isolation in a Mediterranean Sea model has been performed (Taillandier et al., 2006b), and showed the non negligible impact of the assimilation with significant changes in the ocean circulation. In this paper, we further develop this approach but this time in the frame of an operational forecasting system such as MFS. Note that the circulation model used in the previous and present papers is the same (OPA8.2, Madec et al., 1998), but the configurations are different, as detailed in Béranger et al. (2005) for Taillandier et al. (2006b) and in Tonani et al. (2008) for the present study. Differently from the previous study where only trajectory assimilation was considered (Taillandier et al., 2006b), here trajectory data are considered together with the other data of the MFS observing system, i.e. sea surface topography and hydrological profiles. This is an important step for potential improvement of operational predictive systems, given that ARGO floats are an integral and fundamental part of the observing system over the whole ocean and the full exploitation of their information is expected to be of great benefit. Trajectories data are quasi-Lagrangian, i.e. they follow with some approximation the ocean currents, so that their information is directly related to drift velocity. Assimilating them is potentially powerful to improve prediction, but at the same time their compatibility with the other data and with the model itself must be carefully tested.

The present study has three main goals:

- To introduce the assimilation technique that has been developed for the multivariate assimilation of the MFS including the ARGO trajectories, and to prepare for their use in operational mode.
- To verify that the trajectory assimilation is consistent with the assimilation of the other data and with the model mass variables.
- To investigate the specific impact of trajectory assimilation on the various processes and scales of the MFS.

In order to implement the combined assimilation of altimeters, trajectory and profile data, we have used the new formulation of the MFS assimilation scheme that has recently been upgraded to a 3D-var scheme (Dobricic and Pinardi, 2008). A new observation operator is added to the procedure, using a well tested scheme for Lagrangian data analysis (Taillandier et al., 2006a, Taillandier et al., 2008).

The performance of the new assimilation procedure is tested considering the same region (the northwestern Mediterranean Sea) and the same period (winter 2005) that has been previously considered by Taillandier et al. (2006b) for the assimilation of trajectories in isolation (see Figure 1). The choice is primarily dictated by the satisfactory data coverage consisting in four floats in the region during three months. It is still one of the best data coverage up to now in this region for such a long period. As an additional bonus, the comparison with the results of Taillandier et al. (2006b), obtained without the observing system assimilation, will provide additional information on the impact of satellite and TS profile data.

As a first step, the question of internal consistency is considered by testing whether or not the trajectory assimilation alters the misfits with respect to the model variables. This is a relevant and non-trivial question. Given the great number of scales and processes present in the ocean, data compatibility is not always guaranteed, especially for trajectories that sample all the scales of motion and are directly affected by ageostrophic processes. Indeed, the issue of "representativeness", i.e. the impact of spatial and temporal variability of the measured quantities with respect to the scales of the analysis, is one of the great challenges faced by operational oceanography. With the goal of providing a first assessment for the ARGO trajectory assimilation, misfits are computed between observations and their model equivalent for all available data (i.e. SLA from altimeter, TS profiles and trajectories from ARGO floats).

The other assessments, including hydrological sections, net transport through straits, mean circulation and variability, are aimed at quantifying the impact of trajectory assimilation, trying to

identify which processes and scales are mostly influenced. Given the reduced number of independent data available in the considered period, most of the analysis is performed comparing results obtained with and without trajectory assimilation, and considering a qualitative match with respect to historical data. This provides a first insight on the new skills for model predictability and helps identifying the circulation features and the motion scales whose corrections are more effective when assimilating ARGO trajectories. The only set of independent in-situ data available for comparison in the period of interest is given by transport data from current meters in the Corsica Channel (Astraldi and Gasparini, 1992; Astraldi et al., 1999). They have been previously used in Taillandier et al. (2006b), and they are considered here, comparing them with estimates obtained with and without trajectory assimilation. The Corsica Channel is not directly sampled by the floats, but one trajectory is present in the neighborhood and it is able to modify the transport estimates, providing an interesting first quantitative indication on the skills of trajectory assimilation.

The paper is organized as follows. Section 2 describes the integration of ARGO trajectories in the MFS assimilation scheme and its expected impact on the structure of the correction terms. Section 3 deals with the experimental set up while the results are presented in Section 4. Summary and concluding remarks are drawn in Section 5.

2. Method

The integration of ARGO trajectories in the MFS assimilation scheme has been previously investigated in isolation (i.e. assimilating the trajectory data alone) and assessed using a "twin experiment" approach reported in Taillandier and Griffa (2006). The next methodological step considered in the present paper is to effectively consider ARGO trajectories together with the other data information included in the MFS observation system, i.e. SLA from satellite altimeters, vertical TS profiles from ARGO floats, and vertical T profiles from XBT. This is done using a 3D-var scheme recently developed (Dobricic and Pinardi, 2008).

a) Integration of ARGO trajectories in the 3D-var assimilation scheme

The principle of the 3D-var approach is to find iteratively the minimum of the cost function J:

$$J = (x - x^{bck})^T . \mathbf{B}^{-1} . (x - x^{bck}) + (\boldsymbol{H}(x) - y)^T . \mathbf{R}^{-1} . (\boldsymbol{H}(x) - y) \quad (1)$$

where x is the model state vector, x^{bck} is its background or first guess, y the observation vector, $\boldsymbol{H}$ the non-linear observation operator, **B** and **R** the error covariance matrices for x^{bck} and y respectively. The model state variables contained in x are temperature (T), salinity (S), velocity components (**u**) and sea level (η).

In this formalism, the integration of ARGO trajectory observations consists in extending the observation vector y with the positions $\mathbf{r}^{obs}$ acquired at each time t_n when the profilers surface. These new components are assumed independent and associated to Gaussian homogeneous errors. The observation error covariance matrix **R** (Eq.(1)) is then augmented by diagonal terms whose value is equal to the typical uncertainty of ARGO float localization. More details are provided in the description of the experimental set up (Section 3b). The minimization of J at time t_n requires also the model equivalent **r** for float positions. This new quantity is computed by integrating the particle advection equation during the time between previous surfacing time t_b and the present one t_n:

$$d\mathbf{r} / dt = \mathbf{u}(\mathbf{r}(t), t), t \in [t_b, t_n] \quad \text{with } \mathbf{r}(t_b) = \mathbf{r}^{obs}(t_b) \quad (2)$$

This trajectory description is effectively implemented in the 3D-var scheme as a new component of the observation operator $\boldsymbol{H}(x)$. Note that according to the ARGO cycle, the 4D structure of the model state is involved in Eq.(2). The time-varying velocity field **u** is required at the float parking depth during the whole subsurface drift, but also along the vertical to account for shear drift experienced during dives at t_b and resurfacing at t_n. In numerical practice, the trajectory computation of each ARGO float is included in the model simulation, starting from the last observed position ($\mathbf{r}^{obs}(t_b)$ in Eq.(2)), and it is updated with the new observed positions ($\mathbf{r}^{obs}(t_n)$) when the minimization of J is achieved.

Coming back to the description of the 3D-var scheme, the corrected model field, or analysis field, can be written in the incremental variational formalism (Courtier et al., 1994) as:

$$x = x^{bck} + \mathbf{V}.v \quad (3)$$

where v is the so-called control vector and its error covariance matrix **V** built such that $\mathbf{B} = \mathbf{V}.\mathbf{V}^T$. The cost function in Eq.(1) is linearized around x^{bck} and it is re-written in terms of the control vector v such that

$$\delta J = v^T.v + (\mathbf{H}.\mathbf{V}.v - d)^T. \mathbf{R}^{-1}. (\mathbf{H}.\mathbf{V}.v - d) \quad (4)$$

where d is the innovation vector measuring the misfit between the observation vector y and its modeled first guess $\boldsymbol{H}(x^{bck})$, and **H** is the linearized observation operator.

In this formalism, the float position data are included in the innovation vector d at each time t_n they are available. The innovation associated to trajectories is computed as the misfit between the observed positions $\mathbf{r}^{obs}(t_n)$ and the positions $\mathbf{r}^{bck}(t_n)$ simulated inside the background velocity field (Eq.(2)). Then, the minimization of δJ (Eq.(4)) requires an increment for float positions, linearly expressed from the control vector v (Eq.(3)) by the observation operator **H**. This new quantity is computed by integrating a linearized version of the particle advection equation (Eq.(2)) around the background velocity field. The expression of this position increment has been discussed in Taillandier et al. (2006a), and the proposed formulation has been taken up to build **H** and $\mathbf{H}^T$. Overall, the minimization of δJ when fitting position data provides sequential velocity corrections which are used to re-initialize the circulation model at the end of float drifts (Eq.(2)). They represent time-independent (during the observation interval) subsurface velocity structures that determine the observed drifts (with respect to Eq.(2)) when superimposed to the background velocity field.

The practical implementation of the scheme has been detailed in Taillandier and Griffa (2006) and indicated as the “operational procedure” in this previous study. It consists of processing, while the forward integration of the circulation model is operated, a background trajectory and a

background velocity field. A correction of the model state, daily produced by the 3D-var scheme, would include the contribution of a drift if the profiler has surfaced during the day. This contribution is computed considering its observed position, its background trajectory, and the background velocity field during the period of subsurface drift. So the linearity assumption in the 3D-var formulation stands for a time independent correction during a drift period of several days. As discussed in Taillandier et al. (2006b) and hereafter in Section 4a, this is reasonable for the Eulerian velocity correction, given that the Eulerian time scales for mesoscale structures are typically of the order of several days. On the other hand, Lagrangian time scales are expected to be shorter (order of a few days), so that the reconstruction of the Lagrangian path and the associated Lagrangian prediction are expected to be harder to achieve.

b) Heterogeneous observing system

The Mediterranean observing system assimilated in the MFS is composed of data routinely acquired by three types of instrumentations. The ARGO profilers sample the stratification of the water column and return their subsurface drift positions. The XBTs, on the other hand, sample the potential temperature along tracks of ships of opportunity with high spatial resolution but at coarser time resolution (Manzella et al., 2007). The satellite altimeters sample SLA along tracks with a synoptic coverage and a large periodicity (Le Traon et al., 2003), providing information on sea surface topography. So the considered datasets are highly heterogeneous in nature and spatio-temporal distribution. Moreover, they are assimilated sequentially in order to re-initialize the circulation model from a daily analysis. Let us detail the respective contributions of altimeters SLA, TS profiles and subsurface trajectories in the assimilation procedure.

The observations are used by the 3D-var scheme in order to compute the optimal correction of the background model state x^{bck}. As already seen with Eq.(3), this optimization problem is reduced to the estimation of a set of control parameters (vector v). The transformation of the control vector into “physical” model variables is defined by the background error covariances (matrix **V**).

Dobricic and Pinardi (2008) detailed the construction of this **V** that is modeled by a sequence of linear operators such as

$$\mathbf{V} = \mathbf{V}_{uv}.\ \mathbf{V}_{\eta}.\ \mathbf{V}_{H}.\ \mathbf{V}_{V} \qquad (5)$$

$\mathbf{V}_V$ transforms weighting coefficients (control vector v) which multiply vertical EOFs into vertical profiles of temperature and salinity corrections. $\mathbf{V}_H$ applies horizontal covariances of temperature and salinity using a recursive filter that models an isotropic Gaussian correlation pattern for the two passive tracers. $\mathbf{V}_\eta$ estimates the corrections of the sea surface height using a barotropic model forced by the corresponding density perturbations and topography. $\mathbf{V}_{uv}$ estimates the baroclinic part of the velocity correction in geostrophic balance with the surface pressure gradient (from sea surface height correction) and hydrostatic pressure gradient (from density correction).

The adjoint of Eq.(5) transforms the contribution of each observations, into a measure of their sensitivity (in terms of optimal step toward the best linear estimate). In particular, the contribution of ARGO trajectories is projected on the model velocity through $\mathbf{V}_{uv}^{T}$. It impacts on hydrostatic pressure gradients thanks to $\mathbf{V}_{uv}^{T}$, on the model sea level thanks to $\mathbf{V}_{\eta}^{T}$, and finally it changes the horizontal and vertical structure of the mass field thanks to $(\mathbf{V}_H.\mathbf{V}_V)^T$.

Such insight appears particularly interesting given that ARGO floats provide information on both hydrological profile and subsurface drift. Note that the two observations are not truly simultaneous: one is an average over the period of drift, the other is a point measurement at the end of the drift. However, they are analyzed at the same time in the 3D-var scheme. The two contributions document the stratification of the water column at the location of the profile, together with the horizontal gradients of this stratification in the normal direction of the drift at the float parking depth. Isotropic in the case of TS data only, the structure of the correction terms (i.e. the misfit between corrected and background model states) is significantly changed in the presence of trajectory assimilation, according to the new information on horizontal pressure gradients.

This impact on the structure of the correction terms can be investigated considering the corrections of the model mass field in the framework of single observation experiments. Thanks to the experimental set up detailed in Section 3a, three analyses starting from the same initial state and using the same forcing have been performed after one ARGO cycle. In the first analysis, no ARGO data is assimilated. In the second case, only the hydrological profile at the time of analysis is assimilated. In the third case, the drift of ARGO float during the cycle is assimilated together with its hydrological profile. The correction terms associated to the assimilation of TS profile only and to the assimilation of TS profile and drift are then computed as the differences between analyzed model states and model states without assimilation.

Examples are shown in Figure 2 in the neighborhood of an ARGO float drifting along Corsica (see Section 3b). The horizontal structure of the correction term, mapped by misfits on salinity, appears mostly “circular” without trajectory assimilation (Figure 2a). With trajectory assimilation (Figure 2b) it is shaped as a combination of the “dipolar” correction pattern of the horizontal T and S gradients and the “circular” correction pattern of the T and S. The vertical structure of the correction term has similar patterns (Figures 2c-d). Note that horizontal pressure gradients are corrected at the parking depth when assimilating trajectories (Figure 2d). The subsurface corrections are then distributed in the water column according to stratification errors given by the TS profile (Figure 2c) with respect to the geostrophic balance. They are particularly amplified in the upper layer where errors on stratification are significant.

The effects of these error corrections on the overall circulation are assessed in the following sections.

3. Experimental set up

a) Two analyses of the Mediterranean circulation

The results reported in the present study focus on the comparison between two analyses of the Mediterranean circulation focused on the western basin (Figure 1). The first analysis called “OSref”

uses assimilation of observations of SLA and TS profiles, while the second analysis called “OStrj” uses the trajectory data in addition to the SLA and TS observations. Note that the assimilation of SLA uses the new mean dynamic topography calculated by an internal diagnostic of the assimilation system, as described in Dobricic (2005). The 3D-var assimilation scheme described in Dobricic and Pinardi (2008) is used to perform the analysis OSref. The same scheme with the additions detailed in Section 2a is used to perform the analysis OStrj.

The two assimilation experiments start from the same initial state, corresponding to the MFS operational analysis available at January 1 2005. They last for the following 3 months (January 1 – March 31, 2005) in order to cover the whole wintertime period. At the initial time, the assimilation of trajectories is introduced in OStrj and maintained for the whole period, while OSref continues without trajectory assimilation. More precisely in OStrj, the successive analyses operated daily by the 3D-var assimilation scheme will account for trajectory data of the ARGO floats that surfaced the current day. In other words, TS profile and position of each individual float are assimilated in the same analysis with a periodicity given by the float sampling time (every 5 days in the present case).

The model configuration is the one described in Tonani et al. (2008), generated over a meshgrid of resolution 1/16 degree and over 72 geopotential levels (50 in the first 1250m). The atmospheric fluxes of heat and momentum are calculated using interactive bulk formula corrected by satellite SST observations (Pinardi et al., 2003). Background error correlations are computed with vertical time-dependent EOFs as reported in Dobricic et al. (2007), the horizontal correlation radius is kept constant and equal to 30km. Observation error variances are calculated from the experimental uncertainties of each instrumental platform; they are discussed in the next Section 3b for the ARGO trajectories.

b) Four ARGO trajectories in the NW Mediterranean Sea

Four ARGO floats are available in the NW Mediterranean Sea during the period of interest which represents some of the best data coverage up to now in this region for such a long period. The trajectory of the profilers (Figure 1) is indicative of the float displacements at the parking depth of 350m sampled every 5 days (Poulain et al., 2007; http://poseidon.ogs.trieste.it/sire/medargo). Note that for each cycle, the subsurface drift is computed considering the last location before diving and the first location after surfacing. This is clearly an approximation of the real drift, that neglects the effects of surface drift and shear drift during the vertical motion, with consequences on the effective quality of trajectory data. The related uncertainty can be estimated in the range of 1-5km per cycle. This aspect has been discussed and quantified in balance with aliasing related to low sampling in Taillandier and Griffa (2006). More precisely, this numerical study concluded that the influence of such observational errors on the assimilation efficiency did not appear significant in the case of sparse position datasets (few trajectories). A maximal accuracy (corresponding to the lower bound of 1km) is then prescribed for the observational error variance in order to get a representative weight of the sparse trajectory dataset with respect to the other components (SLA and TS profiles).

The four floats cover various parts of the basin. The westernmost float is initially trapped inside a mesoscale eddy then it exits from this structure to drift in the so-called Balearic Current (Font et al., 1988) that flows eastward along the islands. Another float drifts in the central part of the basin, while in the easternmost area, two floats are observed (despite some gaps on position time series) drifting northward into the Ligurian Sea. They document the flow of the Levantine Intermediate Water (LIW) along the western Corsican coast (Millot, 1999). Note that the Northern Current that flows along the continental coast is not sampled by this trajectory dataset.

c) Other datasets

As mentioned in Sections 1 and 2b, the backbone of the MFS observing system includes satellite altimeter, ARGO floats and XBT's. During the considered three month period, no XBT

data were collected in the region of interest, while altimeter data were routinely acquired. The MFS assimilated data therefore include SLA from altimeter and TS profiles from ARGO floats.

In order to assess the impact of adding trajectory assimilation, it would be very useful to have other independent data. Thanks to the continuous monitoring of the exchanges across the Corsica Channel (Astraldi and Gasparini, 1992; Astraldi et al., 1999), time series of the net transport are available in the period. Even though the Corsica Channel (section D in Figure 1) is not directly crossed by the trajectories, one trajectory samples the flow in the neighborhood and it is expected to modify the transport estimates (Taillandier et al., 2006). As a consequence, the comparison between the observed and analyzed transports is considered in the following (Section 4e), providing insights on the trajectory assimilation performance.

The observational estimates of the transport in the Corsica Channel are obtained using a currentmeter mooring located along section D in Figure 1, sampling the current at four levels (50, 100, 300 and 400m). Note that at that location, the Corsica Channel is narrow, with a width of approximately 30km at the surface reducing to 20km at 100m depth and further reducing until the maximum depth of 450m (see Figure 1b in Artale and Gasparini, 1990). The high coherence of the current at different depths suggests the relevance of the barotropic component. Current profile data are extrapolated to estimate the net transport crossing the strait.

In addition to the transport observations, we also use estimates of velocity circulation from SLA to obtain further information on the circulation at the basin scales. SLA from altimeter are assimilated in the model, so that they cannot be considered as independent data. Nevertheless, altimeter data can also be analyzed independently from the model to estimate mean patterns of circulation, and they can used at least to provide qualitative information on velocity patterns. Gridded products are available (Ssalto/Duacs User Handbook, 2006), obtained reconstructing absolute geostrophic velocities from sea surface heights. SLA data are combined with a mean dynamic topography (Rio et al., 2007), in order to restore absolute velocities at a spatial resolution

of 1/8 degree and a temporal resolution of a week. In the present study, velocity averages over the three-month period are computed and used to compare the location and shape of circulation structures analyzed in OSref and OStrj.

d) Diagnostics

Various diagnostics are performed with the aim of comparing the two analyses OSref and OStrj. The first series of diagnostics investigate the observation misfits between each component of the observing system and the associated model quantity. These misfits are routinely available for each daily analysis operated by the 3D-var procedure: the background misfit ($\boldsymbol{H}(x^{bck}) - y$) is computed before minimization, while the analysis misfit ($\boldsymbol{H}(x) - y$) is computed after minimization. A representative value can be computed for each component of the observing system, considering SLA, ARGO TS profiles, and successive positions along ARGO trajectories. An integrated quantity is then computed over the whole assimilation window, considering a root mean square value BmO for the background misfit, and a root mean square value AmO for the analysis misfit. AmO and BmO are computed over a set of 6500 SLA, of 80 hydrological profiles, and 80 final positions after 5-day subsurface drifts for each experiment.

The second series of diagnostics are computed from the daily mean outputs of the model state obtained in OSref and OStrj. They consider regional circulations with the goal of characterizing the impact of the trajectory assimilation on the mean and the variability of the obtained estimates.

First, in order to characterize the seasonal mean stratification and circulation over the region of interest, the mean velocity field is computed at the parking depth of the ARGO floats (350m) over the western Mediterranean and over the three month period. This horizontal point of view is enriched in the vertical considering four relevant sections indicated in Figure 1. The salinity field and the normal component of the absolute velocity field (i.e. assembling geostrophic and ageostrophic components) are computed interpolating along the sections and averaging over the three month period.

Second, in order to characterize the time variability of the analyzed flows, the surface Eddy Kinetic Energy (EKE) averaged over the three month period has been computed for the two analyses OSref and OStrj. The EKE provides a measure of the amplitude of variations which characterize the time evolution of the surface flow. They are induced by assimilated SLA data in geostrophic balance with the barotropic flow, as well as by the complete model dynamics and its response to the atmospheric forcing. The EKE computed from the analysis OSref, called EKEref, constitutes a reference for the overall level of energy. The consistency of the analysis OStrj is then assessed computing its EKE, called EKEtrj, and focusing on the energy inputs generated by the integration of ARGO trajectories. In practice, this is done first of all by computing EKEdiff, given by the difference (EKEtrj – EKEref), that directly documents the changes in the spatial distribution of eddy energy. As a second step, EKEnorm is defined as the absolute value of EKEdiff normalized with respect to the level of the reference EKEref in order to study the consistency of the operated changes due to trajectory integration. Note that EKref and EKEtrj are computed from surface currents analyzed by OSref and OStrj and degraded over the same 1/8° meshgrid. A spatial smoothing filter with an isotropic cut-off radius of 10km is applied to the obtained differences to remove the smallest spots and keep the most representative patterns.

Finally, a comparison is performed between the transport estimates of OSref and OStrj in the Corsica Channel and the transport computed from the independent currentmeter observations. The transport comparison is achieved inside an admissible envelope built from a central value given by current meter data averaged on successive 4-day windows, and by the associated standard deviation inside these 4-day windows. On the other hand, a value of the transport integrated from surface to bottom over the section D is calculated daily from analyzed model outputs during the three-month period. A smoothing filter with a cut-off value of 4 days is applied to the analyzed time series in order to remove high frequency fluctuations.

4. Results

Considering the available data and the numerical approaches detailed in the Sections 2-3, the results reported hereafter are aimed at assessing the self consistency of the Mediterranean Forecasting System when assimilating ARGO trajectories, and at pointing out the corresponding impacts on regional circulations.

a) Comparison of the analyses with the assimilated data

The first assessment focuses on the self-consistency of the 3D-var scheme. It is checked with observation misfits provided by the two experiments, using the diagnostics AmO and BmO defined in Section 3d. The values of AmO and BmO for OSref and OStrj are reported in Table 1 for ARGO trajectory and SLA data, and in Figure 3 for TS profile data.

First of all, the observation misfit related to trajectories appears improved when assimilating trajectories. As shown in Table 1, the BmO value is reduced by 25% between OStrj and OSref. The minimization process appears also accurate as this misfit is dropped down to a value of AmO under 3% of BmO. Note that one might have expected a better value for BmO in OStrj associated to a more persistent adjustment of the modeled trajectories toward the observed ones. This point has already been discussed in Taillandier et al. (2006b), where a similar reduction (around 30%) was obtained for the prediction errors when assimilating trajectories. The general reason is related to the fact that Lagrangian time scales (that are a measure of persistence) are quite short, of the order of a few days. Given the high sensitivity of the trajectories to details of the flow, corrections may appear effective and persistent when ARGO floats move in a regular drift direction, but when the floats are entrained in small scale structures, corrections are significantly less effective.

The second step is to check the values of the observation misfits for the other components of the observing system, i.e. SLA and TS profiles. Again, the observation misfits are significantly reduced by the minimization process for the two experiments OSref and OStrj. When comparing the effect of trajectory assimilation on BmO and AmO, the differences between the two analyses are very small for SLA (Table 1) and temperature (Figure 3a), it is negligible for salinity (Figure

3b). The difference in the temperature misfits shows that, at the position of ARGO floats, the trajectory assimilation has slightly improved the accuracy of temperature analyses above the depth of 300m and has slightly reduced it below. Overall, the trajectory assimilation does not degrade the SLA estimates nor the TS estimates. This is a relevant result, because it indicates that the trajectory assimilation is consistent with the assimilation of the other components (SLA and ARGO profiles) of the observing system.

It is important to note that the observation misfits are computed at the time of analysis, and the trajectory assimilation provides corrections on surface and hydrostatic pressure gradients in a direction orthogonal to the subsurface drift of the floats (as discussed in Section 2b). Hence the impacts on the mass field and on the surface height do not primarily occur at the location of observations, but also (and mainly) in their neighborhood. Such shift on the correction related to trajectory assimilation can be seen in the results of the single observation experiments presented in Section 2b (see Figure 2). At the location of the profile, the differences between the two misfits are very small with respect to the differences obtained in its neighborhood. The correction impact in the neighborhood of the profile will be further investigated in Sections 4b,c considering hydrological sections. Note that there is also little chance to measure the direct influence of trajectory assimilation in the SLA observation misfit because ARGO float trajectories and satellite track intersect very occasionally.

b) Impact on the mean circulation

We consider the mean velocity field at the parking depth of the ARGO floats (350m) that is also characteristic of the LIW circulation. It is shown for the two analyses OSref and OStrj in Figure 4, together with their misfit and with the mean velocity field reconstructed from sea surface topography (see Section 3c). The trajectories are superimposed to the velocity fields to facilitate the interpretation. Since the velocity fields are averaged over three months, a visual close match between trajectories and currents cannot be expected, especially in areas of high variability.

The basin scale circulation in the intermediate layer appears in general good agreement with the circulation schemes reported from field surveys (Millot, 1999; Testor et al., 2005b) for the two analyses. In the Provençal basin (i.e. the northern central part of the area, see Figure 1), a cyclonic circulation is developed along the continental coast from the Ligurian Sea to the Balearic Sea. The return branch meanders between (40°N, 4°E) and (41°N, 8°E) which is identified in the surface layer as the Balearic Front (e.g., Deschamps et al., 1984). In the Algerian basin (i.e. the southern part of the area, see Figure 1), well known features of the regional circulation are represented in the analyses, with a meandering current along the continental coast (e.g. Millot, 1985) and a large anticyclonic eddy similar in both length and velocity scales at all depths to the one observed by Taupier-Letage et al. (2003) offshore the coast at (38°N, 6°E).

In this basin scale point of view, some differences appear between the two analyses (Figure 4c). We can notice that the correction patterns often shape as dipolar structures, such as the one located at (38°N, 6°E), as well as single loop structures, such as the one located at (40.5°N, 3°E). The first type of correction pattern depicts spatial shifts of eddies, while the second type depicts modulations of boundary currents. Their distribution in Figure 4c covers the four trajectory pathways, which indicates the local impact of trajectory assimilation on the intermediate circulation. In addition to this, partial shifts can also be seen away from trajectories, sometimes further than a correlation radius (30km specified for the correction term, see Section 3a), indicating remote corrections. The significance of these corrections cannot be easily assessed at this stage, since they might be due simply to nonlinear propagation of small scale disturbances induced in the initial states by the trajectory assimilation. We will come back on this point in Sections 4d and 5.

In order to see the impact of the trajectory assimilation on the vertical structure of the circulation and on the water masses, (especially the LIW), three hydrological sections crossed by ARGO trajectories are considered (see Figure 1). As detailed in Section 3d, the mean seasonal stratification and the average absolute normal velocities have been computed along these sections

and they are shown in Figures 5-7. In all cases, the main characteristics of stratification and currents are preserved between OSref and OStrj, in agreement with what discussed in Section 4a, and further indicating the consistency of the trajectory data. Nevertheless, specific differences can be seen, especially where the floats cross the sections. The obtained features can be qualitatively compared to what is known from historical datasets in the area, and they are discussed in details in the following Section 4c, considering specific regional analyses. Here, a first brief description is provided at basin scale considering section B that crosses the whole area from south to north.

The hydrological section B (Figure 5) shows the salty Mediterranean waters contrasting with the fresh waters of Atlantic origin, and spreading under the surface layer (deeper than 200m). Their properties are altered when going to the north, with a clear separation marked by a subsurface front. As represented by the section (Figure 5) at 40.5°N, haline properties of the LIW (300-700m depth) are dropped down by at least 0.1PSU. Around this interface (between 39.5°N and 41.5°N), the vertical structure under the Balearic Front is significantly different in the two analyses. The clear cyclonic loop in OSref, located around (40°N, 6°E) where one can see a patch of high salinity (around 39-40.5°N and 300m depth in Figure 5a) is weakened in OStrj with the generation of an eastward branch at 40.2°N. In addition, the general cyclonic pattern around the salty reservoir doming at 42°N is reinforced with trajectory assimilation. The Northern Current is slightly more energetic (especially at surface) in OStrj than in OSref which is consistent with observations carried out by Alberola et al. (1995). Impacts in the mesoscale activity can also be noticed along section B. For example the deepening of the halocline at 38.4°N or the slope of the doming in the northern basin (at 42.1°N) are accentuated in OStrj. They can be linked to the spatial shift of eddies which are crossed by the section B closer to their center.

c) Impact on the regional circulation

Balearic Sea

The current system in the Balearic Sea (see Figure 1 and Figure 4) is composed of the Balearic Current, flowing eastward along the islands, and the Northern Current, flowing westward along the continental slope (Font et al., 1988). This current system can be recognized in cross section A (Figure 6), where the two analyses OSref and OStrj show steep isohalines in the neighborhood of the coasts, indicating the presence of two boundary currents. Main differences can be seen in the Balearic Current as expected, since it is the only current directly sampled by a trajectory (Figure 1). Horizontal salinity gradients at 2.9°E are stronger in OSref (Figure 6a) than in OStrj (Figure 6b). Around this location, absolute velocities, that shape the core of the Balearic Current, appear also more intense and more confined along the coast without trajectory assimilation.

The general structure of the currents across section A is in qualitative agreement with what is known about the area (Pinot and Ganachaud, 1999; Schroeder et al., 2008), even though a quantitative assessment cannot be made, primarily due to data scarcity, but also because of the very high variability, especially concerning the structure and the intensity of the Northern Current (La Violette et al., 1990; Pinot et al., 2002). Historical springtime field survey measurements by Pinot and Ganachaud (1999) show patterns that are similar to the ones in both analyses, while results by Schroeder et al. (2008), taken in April-May 2005 i.e. a few months later than the present analysis, indicate a less intense and less deep current. Note that features of flow reversal has been extensively reported and related to seasonal and mesoscale variability (Pinot et al., 2002; Pascual et al., 2002). The correction in OStrj also goes in the direction of weakening the Balearic Current.

As an interesting side note, we point out that the current along the Balearic Islands was absent in the free (i.e. without assimilation) model run considered in Taillandier et al. (2006b), and it was introduced solely by the trajectory assimilation (see Figure 3 in Taillandier et al., 2006b). Here instead the current is present also in OSref, most likely introduced by SLA assimilation.

The mean LIW circulation at 350m (Figure 4) is similar in OSref and OStrj and it is characterized by an eastward flow, located north of the Balearic Islands, in agreement with the path of the float. The trajectory assimilation tends to slightly slow down and to widen the current, as shown also by the pattern of the differences between OStrj and OSref in Figure 4c, and in agreement with what is shown by the section in Figure 6 or by the surface circulation in Figure 4d. Moreover, the pathway of the LIW, marked in Figure 6 by the subsurface patch of salty waters (higher the 38.48 PSU), appear relocated closer to the coast thanks to trajectory assimilation. In effect, its core is located at 2.85°E in OSref (Figure 6a), at 2.90°E in OStrj (Figure 6b), which is more in agreement with a LIW vein flowing at the coast, as reported by Pinaut and Ganachaud (1999) and Schroeder et al. (2008).

Ligurian Sea

In the Ligurian Sea, the circulation system crossed by the section C (see Figure 1) is also composed of two boundary currents (Béthoux et al., 1982; Béthoux and Prieur, 1983; Sournia et al., 1990; Barth et al., 2005), the Northern Current flowing westward (Sammari et al., 1995) and the current along Corsica that flows northwards. The northward current appears to detach from the Corsica coast in OSref (Figure 4a), joining the loop of the Northern Current without entering the Ligurian Sea, differently from what is shown by the ARGO trajectories. However this branch is also represented in the mean currents reconstructed from sea surface topography (Figure 4d), forming the cyclonic eddy obtained by Barth et al. (2005). Note that in the regional simulation of Barth et al. (2005), this structure is located inside the Ligurian Sea, trapped along the bathymetric contours (see Figure 1), so that the “branching” toward the Provençal basin is located downstream north of Corsica.

The trajectory assimilation tends to relocate eastward this circulation pattern (Figure 4b), even though the high variability in the trajectory paths induces a quite complex feature in the correction (Figure 4c). The branch flowing inside the Ligurian Sea is intensified in OStrj, even though the

cyclonic eddy that blocks the entrance along Corsica is not weakened. A possible explanation would be related to the imbalance of the two forcing responses that drive this regional circulation: a barotropic one governed by a permanent wind curl over the Ligurian Sea, and a baroclinic one governed by the doming reservoir of dense waters that spread eastward until the topographic break (Béthoux and Prieur, 1983; Béthoux et al., 1982). As the latter forcing is weakened because of an under-representation in the model climatology, the main driving force governed by the wind curl acts also in the deeper layers and stabilizes this blocking cyclonic gyre represented in the two analyses (Prieur, personal communication).

As a consequence of this “branching” correction at the southwestern entrance of the Ligurian Sea, the circulation of the LIW is significantly influenced by the trajectory assimilation. As shown in Figure 7, the core of maximum salinity in subsurface, which characterizes the LIW, is well marked in the two analyses, situated along the western Corsican coast and directly sampled by two floats (Figure 1). The vein delimited by the isohaline 38.52 PSU (in dark red color) appears located offshore between 600m and 800m deep in OSref (Figure 7a), while is at the coast between 400m and 700m deep in OStrj (Figure 7b). The location of the LIW core obtained in OStrj is in agreement with sections reported from historical field surveys (Sournia et al., 1990), that obtained a LIW core located at the coast and centered at 500m depth.

Moreover, the trajectory assimilation has an effect on the vertical structure of the velocity (Figure 7). The vein of LIW is located within the core of the boundary current flowing northwestward in OStrj, while in OSref is deeper than the boundary current and located at a more quiescent depth. The pattern depicted by OStrj appears more realistic, because according to historical measurements (Sournia et al., 1990) a persistent branch of LIW would follow the coastal pathway along the western coast of Corsica, without much penetrating the Provençal basin.

Central and Algerian basin

While the ARGO float drifts in the northern part of the Algerian basin, between the Balearic Islands and Corsica from (39.8°N, 5.9°E) to (40°N, 6.3°E) the underlying circulation in Osref shows a strong and tight cyclone (Figure 4a) that is not present in the trajectory. This large cyclonic structure may be considered as a model artefact, since it has never been described by any subsurface float during the dedicated Lagrangian experiments (Testor and Gascard, 2005) nor by any ARGO float which has crossed this area. On the contrary, an anticyclonic circulation was reported by Testor and Gascard (2005) there. Moreover, there is no signature of such a structure in the reconstructed currents by sea surface topography (Figure 4d). The ARGO float was possibly trapped inside a so-called Sardinian eddy, generated along the western Sardinian shelf in the edge of the cyclonic Algerian gyre (Testor and Gascard, 2005; Testor et al., 2005a). This hypothesis is supported by the fact that Sardinian eddies would not show any signature on the surface layer, which is the case looking at the section B (Figure 5 at between 39°5N and 40.5°N). It is also consistent with relatively warmer and saltier waters at intermediate depths revealed by the float profiles there, far offshore.

The information of the trajectory strongly weakens the cyclonic gyre present in the model, which is shown in the mean circulation misfit (Figure 4c) by an energetic anticyclonic pattern extending between (39°N, 7°E) and (40.5°N, 5°E). This correction pattern then influences the mesoscale eddy activity, which is quite significant in the Algerian basin (Taupier-Letage et al., 2003; Testor et al., 2005b). The most visible effect is the shift of the Algerian eddy centered at (38°N, 6°E) (Figure 4c), which has been already mentioned in Section 4b. As the northern component of the dipole is removed (Figure 4b), this eddy tends to be relocated westward in OStrj, which is in agreement with the surface signature given in Figure 4d. Such structure is indeed depicted in the surface layer, as shown in section B at 38.2°N. The increased deepening of the halocline in OStrj (Figure 5b) depicts the translation of the eddy core onto the section location, compared to OSref (Figure 5a) where the section samples the surrounding part of the structure.

The remote effects of the correction appear to impact the reorganisation of the mesoscale features, possibly impacting also the large scale circulation. This could be at least partially peculiar to the Mediterranean, which is an enclosed basin where the mesoscale features appear important and they can even completely reverse the circulation (for instance in the Channel of Sardinia, Ayoub et al., 1998). The quantitative relevance of such remote effects is further addressed in Section 4d.

d) Impact on flow variability

Given the changes induced by trajectory assimilation on the mean flow (e.g. Figure 4c), one can also expect a consequent redistribution of eddy energy due to space and time shifts between OSref and OStrj. At this point, two underlying investigations would be needed when assessing the trajectory integration. The first one is to map this redistribution and locate the energy inputs, while the second one is to quantify the amplitude of the energy inputs and assess their consistency with respect to realistic levels. The third diagnostic described in Section 3d is considered in order to investigate these points.

The surface EKE differences between OSref and OStrj, EKEdiff, are represented in Figure 8a. They can reach an amplitude up to 60 cm^2/s^2 in the Algerian basin where one can find the most intense changes in eddy energy distributions between the two analyses. The amplitudes are smaller in the northern part of the basin but one can notice several patches of magnitude ~10-20 cm^2/s^2. In the same figure, we notice that the eddy energy is input (positive difference) in OStrj along three trajectories (the one in the Balearic Sea and the two in the Ligurian Sea). The three trajectories where turbulent energy levels were low are mainly located on the boundary currents: the assimilation is expected to contribute to a more accurate representation of the variability of these boundary currents. Eddy energy appears removed (negative difference) along the trajectory between Balearic Islands and Sardinia, located in the open ocean inside the model cyclonic gyre centered at (40°N, 6°E). This local energy changes influence the intensity of the neighboring structures,

particularly in the southern central area (tripolar shapes at (39°N, 6.5°E)) and more slightly at the entrance of the Balearic Sea (41°N, 4°E) or in the Ligurian Sea (43°N, 8°E).

The energy changes obtained along trajectories appear more clearly in the normalized EKE, EKEnorm, shown in Figure 8b. As it can be seen, relative differences exceed 50% of the reference value in regions directly sampled by the floats. On the other hand, remote changes away from the trajectories are relatively suppressed especially in the southern central area characterized by high eddy energy levels. This suggests that significant changes are mostly local, i.e. along the trajectories, while the remote changes appears less significant and likely to be related to nonlinear propagation of relatively small disturbances. Note that this is in agreement with results of previous numerical studies on the sensitivity to the number of active ARGO floats (Taillandier and Griffa, 2006), in which it was shown that a basin-wide correction occurs for large trajectory datasets (more than 10 floats in the western Mediterranean), while for sparse datasets (less than 5 floats) the contribution is mostly local.

e) Transport through the Corsica Channel

The transport computed in the Corsica Channel (through the section D, see Figure 1) from OSref and OStrj is compared with in-situ measurements in Figure 9. We recall that one ARGO trajectory is present in the neighborhood of this section (see Figure 1), even though it does not directly crosses the Corsica Channel. The influence of trajectory assimilation at the strait location is clearly marked in the mean circulation (Figure 4c) as well as in its variability (patches around (43°N, 8°E) in Figure 8).

The observation time series (black line in Figure 9) shows the occurrence of significant fluctuations during the considered period, reaching minimum values of 0.7Sv and maximum values of 1.6Sv. The associated standard deviation for the 4-day average (gray envelope) also fluctuates significantly up 0.3Sv. The mean value over the period (straight black line) is of 1.12Sv directed northward through the strait. The OSref time series (blue line) appear to follow quite closely the

observation oscillations and stay inside the gray envelope at least up to mid February. Its phase appears also quite consistent with observations up to February 15th. After that, a phase shift (~3-7 days) can be observed, with the OSref results tending to lag behind the observations, so that the analyzed transports leave the observation envelope. After March 10, a more significant departure from observation is observed, with the observations showing a strong decrease in the northward transport that is not present in OSref. This is reflected also on the mean transport value that is higher for OSref, 1.19Sv (straight blue line).

The results for OStrj (red line) maintain close to OSref up to the end of February, when the presence of a nearby trajectory starts to influence more strongly the transport. At the beginning of March, Ostrj appears to underestimate the observed transport more than Osref. Soon after that, though, OStrj shows a decrease in transport that is not present in OSref and that is more consistent with the observations, even though the difference with the observations is still significant. The mean transport over the period is lower than for OSref and it coincides almost exactly with the one of the observations, 1.11Sv (red straight line). This effect is shown also by the differences in the mean circulation (Figure 4c), indicating a southward difference flow in the Channel. The decrease of the mean transport in OStrj is likely to be related to a better estimation during the period (March 10-31) when one ARGO profiler drifts in the neighborhood of the strait, but it might also benefit of the accentuated underestimation during the initial March period. Overall, the assimilation of the trajectories, while maintaining the basic transport features, appears to improve the results of OSref when a trajectory is nearby.

As an interesting side note, we qualitatively compare the results in Figure 9 with the analogous results obtained in Taillandier et al (2006b) (Figure 5 of the article) where a free run (i.e. with no assimilation) was considered as reference and the assimilation of trajectories in isolation was added. Overall, the results in Taillandier et al (2006b) appear significantly less energetic, therefore indicating that the assimilation of the MFS observing system significantly improves the

realism of the energy level. Also, the free run in Taillandier et al. (2006b) was underestimating the mean northward transport, and the trajectory assimilation contributed to intensify it. In the present case, the inverse is observed, with a reference overestimating the mean northward transport, and the trajectory assimilation acting as to reduce the transport. This contributes to show the consistency of the transport correction in presence of trajectory assimilation. Finally, we observe that the shift noticed in Figure 9 between the observed fluctuations and the analyzed ones is also present and reinforced in Taillandier et al (2006b). This suggests that the shift could be due to an inherent delay in the model answer to atmospheric forcing. More investigations will be needed to assess this point.

5. Summary and concluding remarks

This study reports the first results obtained assimilating simultaneously ARGO trajectories together with their profile data and satellite altimeters' SLA. It has been lead using the Mediterranean Forecasting System in which ARGO float position data have been integrated in the observing system. Short term analyses have been performed to identify the contribution and the consistency of such Lagrangian subsurface observations.

Regarding the self consistency of the new forecasting system, the statistics of the misfits between observations and model forecast and analysis show that the trajectory assimilation does not deteriorate the analysis obtained assimilating ARGO profiles and SLA. Rather, the trajectory assimilation contributes to refine the structure of the correction term: the isotropic correction provided by hydrological profiles is improved by a correction of the TS horizontal gradient (hence of the hydrostatic pressure gradient) in a direction orthogonal to the drift of the floats. As a consequence, the analysis benefits of a more accurate description of the boundary currents sampled by ARGO trajectories, because the structure of correction term accounts for the anisotropic pattern of hydrostatic pressure gradients (mainly in the cross-shore direction). Note that this information is not well resolved by the other components of the observing system for a regional environment such as the Mediterranean Sea.

Regarding the impacts of trajectory assimilation, the sensitivity study on the seasonal mean circulation and its variability shows significant changes at locations sampled by trajectories. They can be quite intense in coastal areas where turbulent energy levels are relatively low in the analysis of reference, and where eddy energy inputs appear significant (in the Balearic Sea) in consequence of the information on hydrostatic pressure gradients brought by the trajectories.

The correction patterns obtained in the sensitivity study have been detailed at the regional level and qualitatively compared to historical datasets. The width and the intensity of boundary currents sampled by trajectories appear qualitatively improved (along the Balearic Islands) as well as the location of their branching toward the interior basin (at the entrance of the Ligurian Sea). The distribution of the water masses is also qualitatively improved, especially for the LIW whose pathway at the coast and at appropriate depth appears in better agreement with historical datasets. The results of the analyses have also been compared with independent observations of transport in the Corsica Channel, obtained from current meter data (Astraldi and Gasparini, 1992). The Corsica Channel is not directly crossed by any float, but there is one trajectory nearby whose assimilation influences the transport estimates. Overall, trajectory assimilation is found to improve the comparison with observed transport, even though the difference with the observations is still significant.

The results obtained in this short-term analysis motivate further investigations and applications. An interesting question, that is common also to other sparse data sets, is what are the relevance and the impact of remote corrections occurring away from the trajectories. A possible hypothesis is that they might act as to rearrange the mesoscale, influencing also the large scale circulation. An alternative hypothesis, instead, is that they do not induce significant changes on the system state, but rather they fall in the envelope of uncertainty of the solution. In other words, they can be seen as nonlinear propagations of small disturbances of the solution. The results obtained in this paper by normalizing the variability induced by the corrections tend to support this last

hypothesis. More robust validations are needed in the future, and at least two possible approaches can be foreseen. First, ensemble simulations can be considered to study the effectiveness and the stability of remote correction patterns, for instance considering small scale perturbations of the initial state of the system and their evolution envelope. Second, longer term analyses will be performed over the whole Mediterranean circulation taking into account float trajectories since 1997 when profilers started to be deployed (Testor et al., 2005b). This will provide more robust and extended statistics.

In the planning of future deployments of ARGO floats in the Mediterranean Sea, Observing System Simulation Experiments will be performed to quantify the minimum number of trajectories needed to provide basin-wide corrections, i.e. to efficiently constrain the remote impacts of local corrections in the framework of an operational system. A first numerical study by Taillandier and Griffa (2006) assessed the minimum spatial coverage of trajectories within a three month period in the western Mediterranean. Further studies are needed using assimilation experiments of longer duration and including the assessment of temporal coverage requirements.

As the main features of the circulation are driven by boundary currents, a more accurate characterization of their dynamics obtained using ARGO trajectories would help to refine the energetic balances associated to the thermohaline circulation. Note also that a particular effort needs to be done for the representation of the Northern Current and the undercurrent LIW circulation over the Provençal basin, by acting on the climatological initialization to settle a consistent deep water reservoir, and by acting on the observing system using dedicated autonomous platforms such gliders (Niewiadomska et al., 2008) or instrumented moorings.

The present methodology and associated skills open perspective avenues toward the integration of trajectory data in forecasting systems operating in other regions, given that ARGO floats are an integral and fundamental part of the world oceans observing system (reaching nowadays 3000 profilers deployed). So, the full exploitation of their information is expected to be

of great benefit for prediction. Longer term perspectives are also opened considering other in-situ automated quasi-Lagrangian platforms such as surface drifters and gliders that would also provide fruitful information for an improved representation of mesoscales in future re-analyses and forecasts.

Acknowledgments

We would like to acknowledge Karine Béranger and Louis Prieur for fruitful discussions, as well as Pierre-Marie Poulain and the MedArgo team that deployed the profilers and processed the data. The altimeter products were provided by Ssalto/Duacs and distributed by Aviso with the kind support of Stéphanie Guinehut from CLS. VT was funded by the French ANR under the grant LIVINGSTONE. AG was funded by ONR, grant N00014-05-1-0094. We acknowledge the anonymous reviewers for their thorough reading and constructive criticisms.

References

Alberola, C., C. Millot, and J. Font (1995). On the seasonal and mesoscale variabilities of the Northern Current during the PRIMO-0 experiment in the western Mediterranean Sea. *Oceanologica Acta*, 18, 163-192.

Artale, V., and G.P. Gasparini (1990). Simultaneous temperature and velocity measurements of the internal wave field in the Corsican Channel (Eastern Ligurian Sea). *Journal of Geophysical Research*, 95, 1635-1645.

Astraldi, M., and G.P. Gasparini (1992). The seasonal characteristics of the circulation in the north Mediterranean Basin and their relationship with the atmospheric-climatic conditions. *Journal of Geophysical Research*, 97, 9531-9540.

Astraldi, M., M. Balopoulos, J. Candela, J. Font, M. Gacic, G.-P. Gasparini, B. Manca, A. Theocharis, and J. Tintore (1999). The role of straits and channels in understanding the characteristics of Mediterranean circulation. *Progress in Oceanography*, 44, 65-108.

Ayoub, N., P.Y. Le Traon, and P. De Mey (1998). A description of the Mediterranean surface variable circulation from combined ERS-1ERS-1 and TOPEX/POSEIDON altimetric data. *Journal of Marine Systems*, 18, 3-40.

Barth, A., A. Alvera-Azcarate, M. Rixen, and J.M. Beckers (2005). Two-way nested model of mesoscale circulation features in the Ligurian Sea. *Journal of Marine Systems*, 66, 171-189.

Béranger, K., L. Mortier, and M. Crépon (2005). Seasonal variability of water transport through the straits of Gibraltar, Sicily and Corsica, derived from a high-resolution model of the Mediterranean circulation. *Progress in Oceanography*, 2-4, 341-364.

Béthoux, J.P., L. Prieur, and F. Nyffeler (1982). The water circulation in the north-western Mediterranean Sea, its relations with wind and atmospheric pressure. in: Nihoul, J.C.J. (Ed.). Hydrodynamics of semi-enclosed seas: Proceedings of the 13th International Liège Colloquium on Ocean Hydrodynamics. *Elsevier Oceanography Series*, 34, 129-142.

Béthoux, J.P., and L. Prieur (1983). Hydrologie et circulation en Méditerranée nord-occidentale. *Pétrole Technique*, 299, 25-34.

Bouzinac, C., J. Font and C. Millot (1999). Hydrology and currents observed in the channel of Sardinia during the PRIMO-1 experiment from November 1993 to October 1994. *Journal of Marine Systems*, 20, 333-355.

Buongiorno Nardelli, B., G. Larnicol, E. D'Acunzo, R. Santoleri, S. Marullo, and P.Y. Le Traon (2003). Near real time SLA and SST products during 2 years of MFS pilot project : processing, analysis of the variability and of the coupled patterns. *Annales Geophysicae*, 21, 103-121.

Courtier, P., J.-N. Thépaut, and A. Hollingsworth (1994). A strategy for operational implementation of 4D-Var, using an incremental approach. *Quarterly Journal of Royal Meteorological Society*, 120, 1367–1388.

Crépon M., L. Wald, and J.M. Longuet (1982). Low frequency waves in the Ligurian Sea during December 1977. *Journal of Geophysical Research*, 87, 595-600.

Demirov, E., and N. Pinardi (2007). On the relationship between the water mass pathways and eddy variability in the Western Mediterranean Sea. *Journal of Geophysical Research*, 112, C02024.

Deschamps, P.Y., R. Frouin, and M. Crépon (1984). Sea surface temperatures of the coastal zones of France observed by the HCMM satellite. *Journal of Geophysical Research*, 89, 81238149.

Dobricic, S. (2005). New mean dynamic topography of the Mediterranean calculated from assimilation system diagnostics, *Geophysical Research Letters*, 32, L11606.

Dobricic, S., N. Pinardi, M. Adani, A. Bonazzi, C. Fratianni, and M. Tonani (2005). Mediterranean Forecasting System: An improved assimilation scheme for sea-level anomaly and its validation. *Quarterly Journal of the Royal Meteorological Society*, 131, 3627-3642.

Dobricic, S., N. Pinardi, M. Adani, M. Tonani, C. Fratianni, A. Bonazzi, and V. Fernandez (2007). Daily oceanographic analyses by the Mediterranean basin scale assimilation system. *Ocean Science*, 3, 149-157.

Dobricic, S., N. Pinardi, P. Testor, and U. Send. Data assimilation of glider observations in the Ionian Sea (Eastern Mediterranean): a study of the path of the Atlantic Ionian Stream. *Ocean Modelling*, in revision.

Dobricic, S., and N. Pinardi (2008). An oceanographic three-dimensional variational data assimilation scheme. *Ocean Modelling*, 22, 3-4, 89-105.

Font, J., J. Salat, and J. Tintoré (1988). Permanent features of the circulation in the Catalan Sea. *Oceanologica Acta*, 9, 51-57.

Ide, K., L. Kuznetsov, and C.K.R.T. Jones (2002). Lagrangian data assimilation for point vortex systems. *Journal of Turbulence*, 3, 53-59.

Ishikawa, Y.I., T. Awaji, and K. Akimoto (1996). Successive correction of mean sea surface height by the simulatneous assimilation of drifting buoys and altimetric data. *Journal of Physical Oceanography*, 26, 2381-2397.

Kamachi, M., and J.J. O'Brien (1995). Continuous assimilation of drifting buoy trajectories into an equatorial Pacific Ocean model. *Journal of Marine Systems*, 6, 159–178.

Kuznetsov, L., K. Ide, and C.K.R.T. Jones (2003). A method for assimilation of lagrangian data. *Monthly Weather Review*, 131, 2247–2260.

LaViolette, P. E., J. Tintoré, and J. Font (1990). The surface circulation of the Balearic Sea, *Journal of Geophysical Research*, 95, 1559–1568.

Le Traon, P.Y., F. Nadal, and N. Ducet (2003). An improved mapping method of multisatellite altimeter data. *Journal of Atmospheric and Oceanic Technology*, 15, 522-533.

Madec, C., F. Lott, P. Delecluse, and M. Crépon (1996). Large scale preconditioning of deep water formation in the north-western Mediterranean sea. *Journal of Physical Oceanography*, 26, 1393-1408.

Madec, G., P. Delecluse, M. Imbard, and C. Levy (1998). OPA8.1 Ocean general Circulation Model reference manual. Note du pôle de modélisation, Institut Pierre-Simon Laplace, France.

Manzella, G.M.R., F. Reseghetti, G. Coppini, M. Borghini, A. Cruzado, C. Galli, I. Gertman, T. Gervais, D. Hayes, C. Millot, A. Murashkovsky, E. Özsoy, C. Tziavos, Z. Velasquez, and G. Zodiatis (2007). The improvements of the ships of opportunity program in MFSTEP. *Ocean Science*, 3, 245-258.

Mariano, A.J., T.M. Chin, and T.M. Ozgokmen (2003). Stochastic boundary conditions for modeling of coastal flows. *Geophysical Research Letters*, 30, GL016972.

Marullo, S., B. Buongiorno Nardelli, M. Guarracino, and R. Santoleri (2007). Observing the Mediterranean Sea from space: 21 years of pathfinder-AVHRR sea surface temperatures (1985-2005): re-analysis and validation. *Ocean Science*, 3, 299-310.

Millot, C. (1985). Some features of the Algerian current. *Journal of Geophysical Research*, 90, 7169-7176.

Millot, C. (1999). Circulation in the Western Mediterranean Sea. *Journal of Marine Systems*, 20, 423-442.

Molcard, A., A. Griffa, and T.M. Ozgokmen (2005). Lagrangian data assimilation in multi-layer primitive equation ocean models. Journal of Atmospheric and Oceanic Technology, 22, 70–83.

Molcard, A., L.I. Piterbarg, A. Griffa, T.M. Ozgokmen, and A.J. Mariano (2003). Assimilation of drifter positions for the reconstruction of the eulerian circulation field. *Journal of Geophysical Research*, 108, 3056.

Niewiadomska, K., H. Claustre, L. Prieur, and F. d'Ortenzio (2008). Submesoscale physical-biogeochemical coupling across the Ligurian current (northwestern Mediterranean) using a bio-optical glider. *Limnology and Oceanography*, 53, 2210-2225.

Nittis, K., C. Tziavos, R. Bozzano, V. Cardin, Y. Thanos, G. Petihakis, M.E. Schiano, and F. Zanon (2007). The M3A multi-sensor buoy network of the Mediterranean Sea. *Ocean Science*, 3, 229-243.

Nodet, M. (2006). Variational assimilation of Lagrangian data in oceanography. *Inverse Problems*, 22, 245-263.

Ozgokmen, T.M., A. Griffa, L.I. Piterbarg, and A.J. Mariano (2000). On the predictability of the Lagrangian trajectories in the ocean. *Journal of Atmospheric and Oceanic Technology*, 17, 366–383.

Pascual, A., B. Buongiorno Nardelli, G. Larnicol, M. Emelianov, and D. Gomis (2002). A case of an intense anticyclonic eddy in the Balearic Sea (western Mediterranean). *Journal of Geophysical Research*, 107, 3183.

Pinardi, N., I. Allen, E. Demirov, P. De Mey, G. Korres, A. Lascaratos, P.-Y. Le Traon, C.Maillard, G. Manzella, and C. Tziavos (2003). The Mediterranean ocean forecasting system: first phase of implementation (1998-2001). *Annales Geophysicae*, 21, 3-20.

Pinot, J.M., J.L. Lopez-Jurado and M. Riera (2002). The CANALES experiment (1996-1998). Interannual, seasonal, and mesoscale variability of the circulation in the Balearic Channels. *Progress in Oceanography*, 55, 335-370.

Pinot, J.-M., and A. Ganachaud (1999). The role of winter intermediate wters in the spring-summer circulation of the Balrearic Sea. 1. Hydrography and inverse box modeling. *Journal of Geophysical Research*, 104, 29843-29864.

Poulain, P.M., R. Barbanti, J. Font, A. Cruzado, C. Millot, I. Gertman, A. Griffa, A. Molcard, V. Rupolo, S. Le Bras, and L. Petit de la Villeon (2007). MedARGO: a drifting profiler program in the Mediterranean Sea. *Ocean Science*, 3, 379-395.

Puillat, I., I. Taupier-Letage, and C. Millot (2002). Algerian eddies can span near three years. *Journal of Marine Systems*, 31, 245-259.

Rio, M.-H., P.-M. Poulain, A. Pascual, E. Mauri, G. Larnicol, and R. Santoleri (2007). A Mean Dynamic Topography of the Mediterranean Sea computed from altimetric data, in-situ measurements and a general circulation model. *Journal of Marine Systems*, 65, 484-508.

Sammari, C., C. Millot, and L. Prieur (1995). Aspects of the seasonal and mesoscale variabilities of the Northern Current in the western Mediterranean Sea inferred from the PROLIG-2 and PROS-6 experiments. *Deep-Sea Research Part 1*, 42, 893-917.

Schroeder K., V. Taillandier, A. Vetrano, and G.-P. Gasparini (2008). The circulation of the Western Mediterranean Sea in spring 2005 as inferred from observations and from model outputs. *Deep-Sea Research Part 1*, 55, 947-965.

Sournia, A., J.M. Brylinski, S. Dallot, P. Le Corre, M. Leveau, L. Prieur, and C. Froget (1990). Fronts hydrologiques au large des côtes françaises: les sites-ateliers du programme Frontal. *Oceanologica Acta*, 13, 413-438.

Ssalto/Duacs User handbook (2006). (M)SLA and (M)ADT near-real time and delayed time products. *CLS-DOS-NT-06.034*.

Taillandier, V., A. Griffa, P.M. Poulain, R. Signell, J. Chiggiato and S. Carniel (2008). Variational analysis of drifter positions and model outputs for the reconstruction of surface currents in the Central Adriatic during fall 2002. *Journal of Geophysical Research*, 113, JC004148.

Taillandier, V., A. Griffa, and A. Molcard (2006a). A variational approach for the reconstruction of regional scale Eulerian velocity fields from Lagrangian data. *Ocean Modelling*, 13, 1-24.

Taillandier, V., A. Griffa, P.-M. Poulain, and K. Béranger (2006b). Assimilation of ARGO float positions in the North Western Mediterranean Sea and impact on ocean circulation simulations. *Geophysical Research Letters*, L11604.

Taillandier, V., and A. Griffa (2006). Implementation of a position assimilation method for ARGO floats in a Mediterranean Sea OPA model and twin experiment testing. *Ocean Science*, 2, 223-236.

Taupier-Letage, I., I. Puillat, P. Raimbault, and C. Millot (2003), Biological response to mesoscale eddies in the Algerian Basin. *Journal of Geophysical Research*, 108, 3245-3267.

Testor, P., K. Béranger, and L. Mortier (2005a). Modeling the deep eddy field in the south-western Mediterranean: the life cycle of Sardinian eddies. *Geophysical Research Letters*, 32, L13602.

Testor, P., U. Send, J.C. Gascard, C. Millot, I. Taupier-Letage, and K. Béranger (2005b). The mean circulation of the southwestern Mediterranean Sea - the Algerian Gyres. J*ournal of Geophysical Research*, 110, C11017.

Testor, P., and J.-C. Gascard (2005). Large scale flow separation and mesoscale eddy formation in the Algerian Basin. *Progress in Oceanography*, 66, 211-230.

Testor, P., and J.-C. Gascard (2006). Post convection spreading phase in the north-western Mediterranean Sea. *Deep Sea Research Part I*, 53, 869-893.

Tonani, M., N. Pinardi, S. Dobricic, I. Pujol and C. Fratianni (2008). A high resolution free surface model of the Mediterranean Sea. *Ocean Science*, 4, 1-14.

Figure caption list

Figure 1: Trajectories of four ARGO floats inside the NW Mediterranean. The four sections of the Balearic Sea (A), the Algero-Provençal basin (B), the Ligurian Sea (C), and Corsica Channel (D) are also indicated in straight lines superimposed on the isobaths 500m, 1000m, 2000m.

Figure 2a: Structure of the correction term provided by single observation experiments in the neighborhood of Corsica. Difference between the salinity (in PSU) analyzed with a TS profile located at (42°N, 8°E) and the background salinity field at 200m; the ARGO drift at 350m is superimposed.

Figure 2b: Same as Figure 2a considering the analysis of the same TS profile plus the subsurface drift.

Figure 2c: Same as Figure 2a along a zonal section at 42°N.

Figure 2d: Same as Figure 2b along a zonal section at 42°N.

Figure 3: Root mean square of temperature misfits (^{o}C, left panel) and salinity misfits (PSU, right panel) in the period January-March 2005. The two diagnostics AmO (thin lines) and BmO (bold lines), defined in Section 3d, are represented in full line for OSref (without trajectory assimilation), and in dashed line for OStrj (with trajectory assimilation).

Figure 4a: Mean circulation at 350m computed from OSref. The velocities (in cm/s) are superimposed on the amplitude (in cm/s) of the currents, as well as the four ARGO trajectories and the four sections.

Figure 4b: Same as Figure 4a for the mean circulation at 350m computed from OStrj.

Figure 4c: Same as Figure 4a for the difference between the two flows at 350m (OStrj minus OSref).

Figure 4d: Same as Figure 4a for the mean circulation computed from currents reconstructed by sea surface topography (Aviso product).

Figure 5a: Mean stratification along the section B (Algero-Provençal basin). Salinity (in PSU) extracted daily from the analysis OSref, and averaged during the period January 1 – March 31, 2005. Contours: absolute velocities normal to the section (in cm/s, every 5cm/s) averaged over the same period.

Figure 5b: Same as Figure 5a for the analysis OStrj.

Figure 6a: Same as Figure 5a along the section A (Balearic Sea).

Figure 6b: Same as Figure 6a for the analysis OStrj.

Figure 7a: Same as Figure 5a along the section C (Ligurian Sea). Contours: absolute velocities normal to the section (in cm/s, every 1cm/s) averaged over the same period.

Figure 7b: Same as Figure 7a for the analysis OStrj.

Figure 8a: Comparison of the mean EKE as obtained by the two analyzed surface flows over the period January 1 – March 31, 2005. EKEdiff, computed as difference between OStrj and OSref (in cm^2/s^2), regridded at a 1/8 degree resolution and low-pass filtered with a cut-off radius of 10km. The four ARGO trajectories are also superimposed.

Figure 8b: Same as Figure 8a for EKEnorm, computed as absolute EKE difference normalized by the EKE of reference.

Figure 9: Evolution of the net transport crossing the section of the Corsica Channel. Plot in blue corresponds to OSref, in red to OStrj, and in black to the independent observation by moored current meter. The envelope of admissible values with respect to the standard deviation of the observed transports is indicated in grey. The mean transports over the period are also plotted by the straight lines. The time-series from the two analyses have been low-pass filtered with a cut-off period of 4 days.

Table 1: Root mean square of SLA misfits and ARGO trajectory misfits in the period January-March 2005. The two diagnostics AmO and BmO defined in Section 3d have been performed in OSref (without trajectory assimilation) and OStrj (with trajectory assimilation).

		BmO	AmO
ARGO trajectories	OSref	34.48 km	-
	OStrj	26.72 km	780 m
Sea level anomalies	OSref	3.90 cm	2.46 cm
	OStrj	3.91 cm	2.45 cm

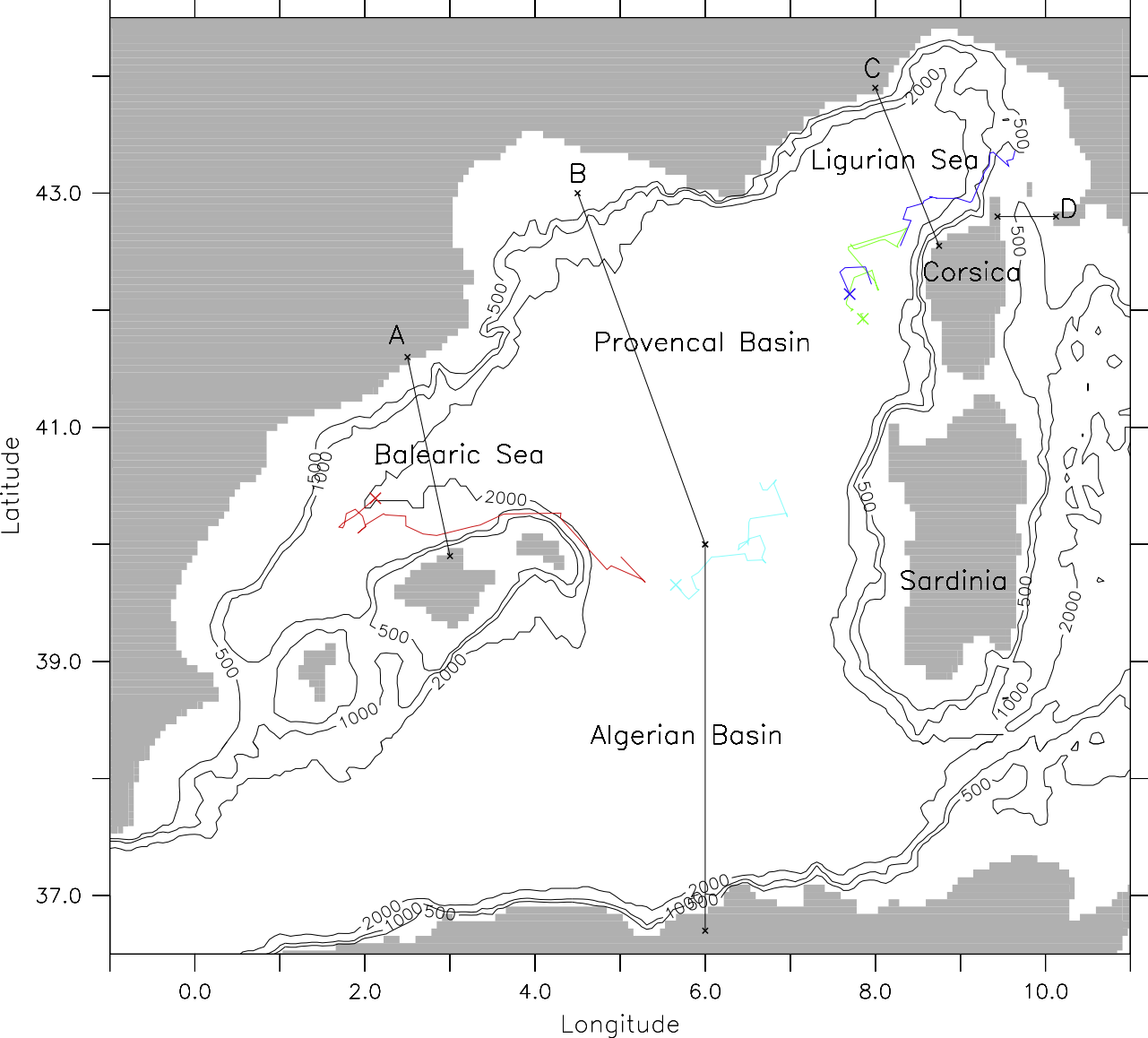
A
B
C
D
Ligurian Sea
Provencal Basin
Balearic Sea
Corsica
Sardinia
Algerian Basin
500
1000
2000
43.0
41.0
39.0
37.0
Latitude
0.0
2.0
4.0
6.0
8.0
10.0
Longitude

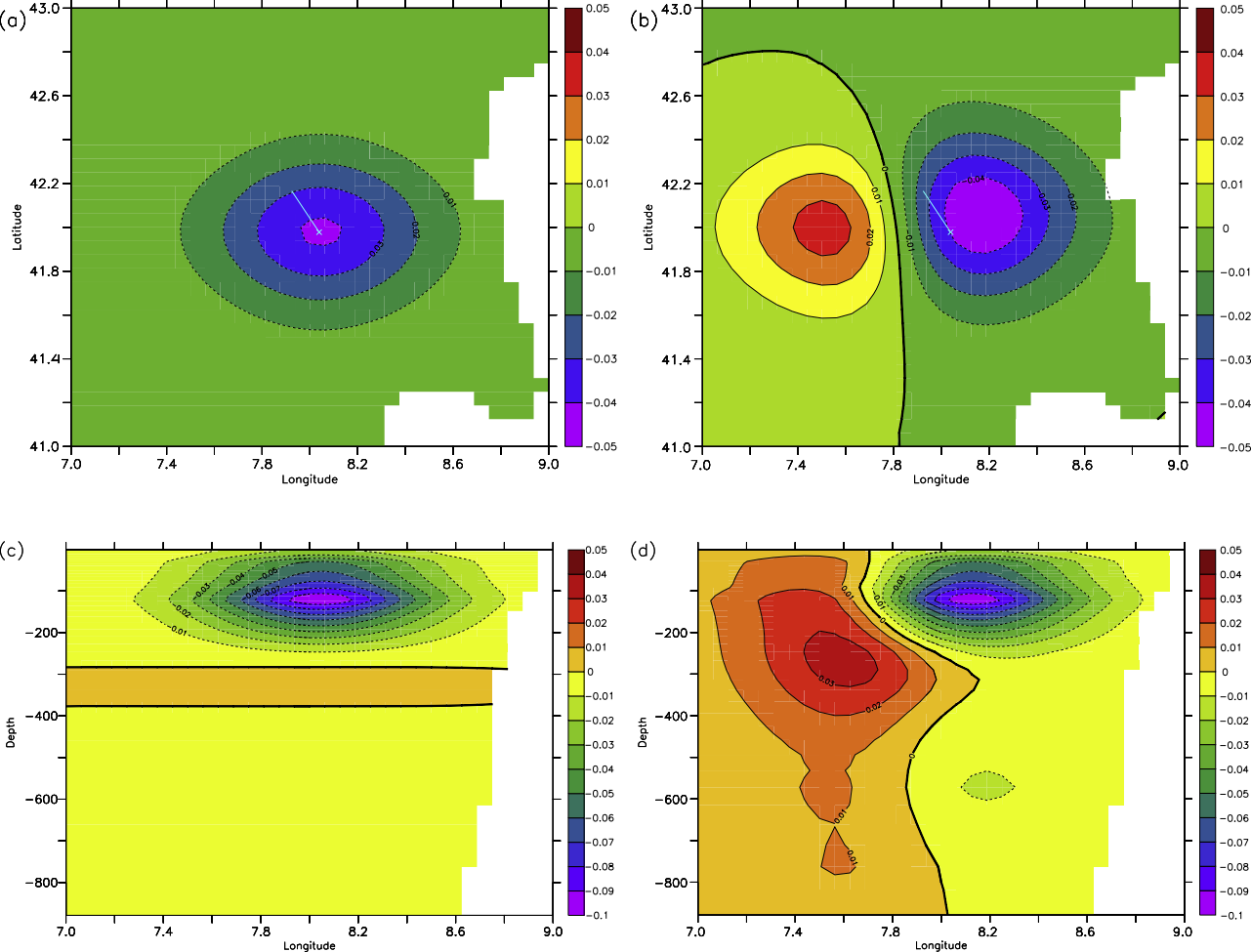
(a)
(b)
(c)
(d)
Latitude
Longitude
Depth
43.0
42.6
42.2
41.8
41.4
41.0
7.0
7.4
7.8
8.2
8.6
9.0
−200
−400
−600
−800
0.05
0.04
0.03
0.02
0.01
0
−0.01
−0.02
−0.03
−0.04
−0.05
−0.06
−0.07
−0.08
−0.09
−0.1

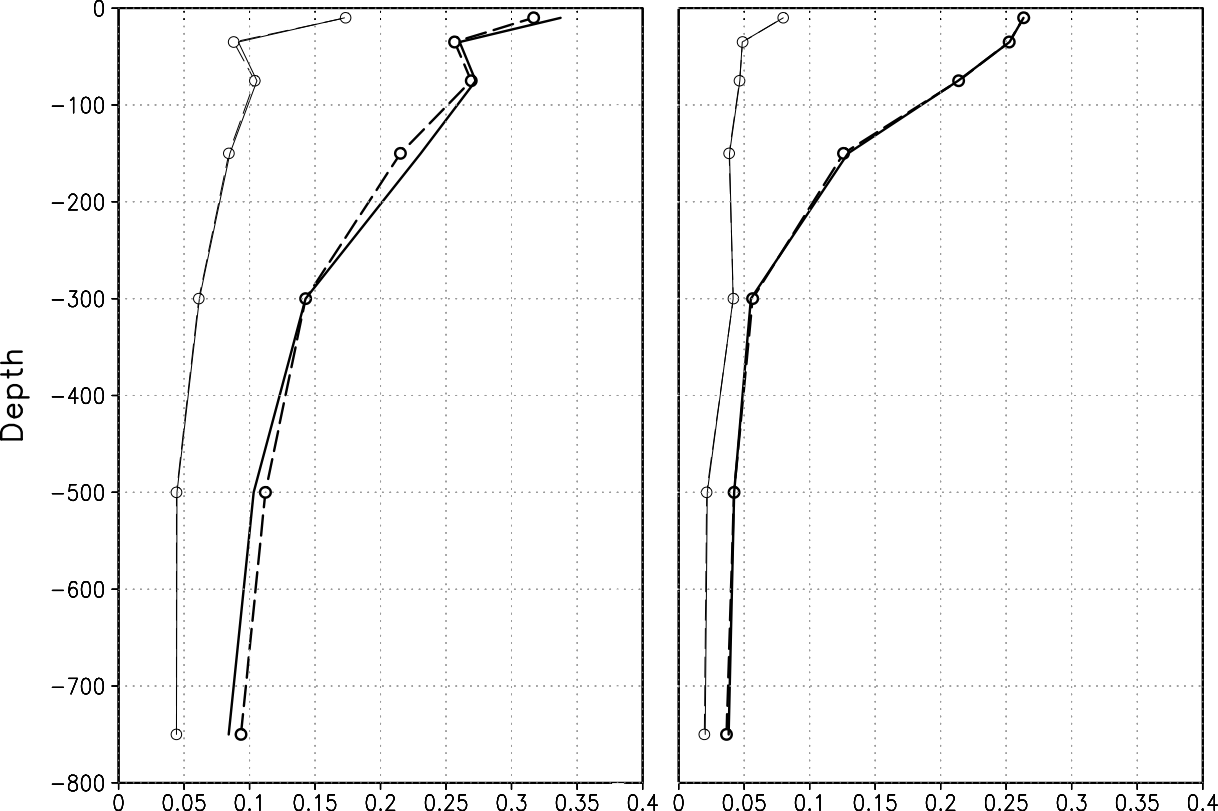
Depth
0
−100
−200
−300
−400
−500
−600
−700
−800
0
0.05
0.1
0.15
0.2
0.25
0.3
0.35
0.4

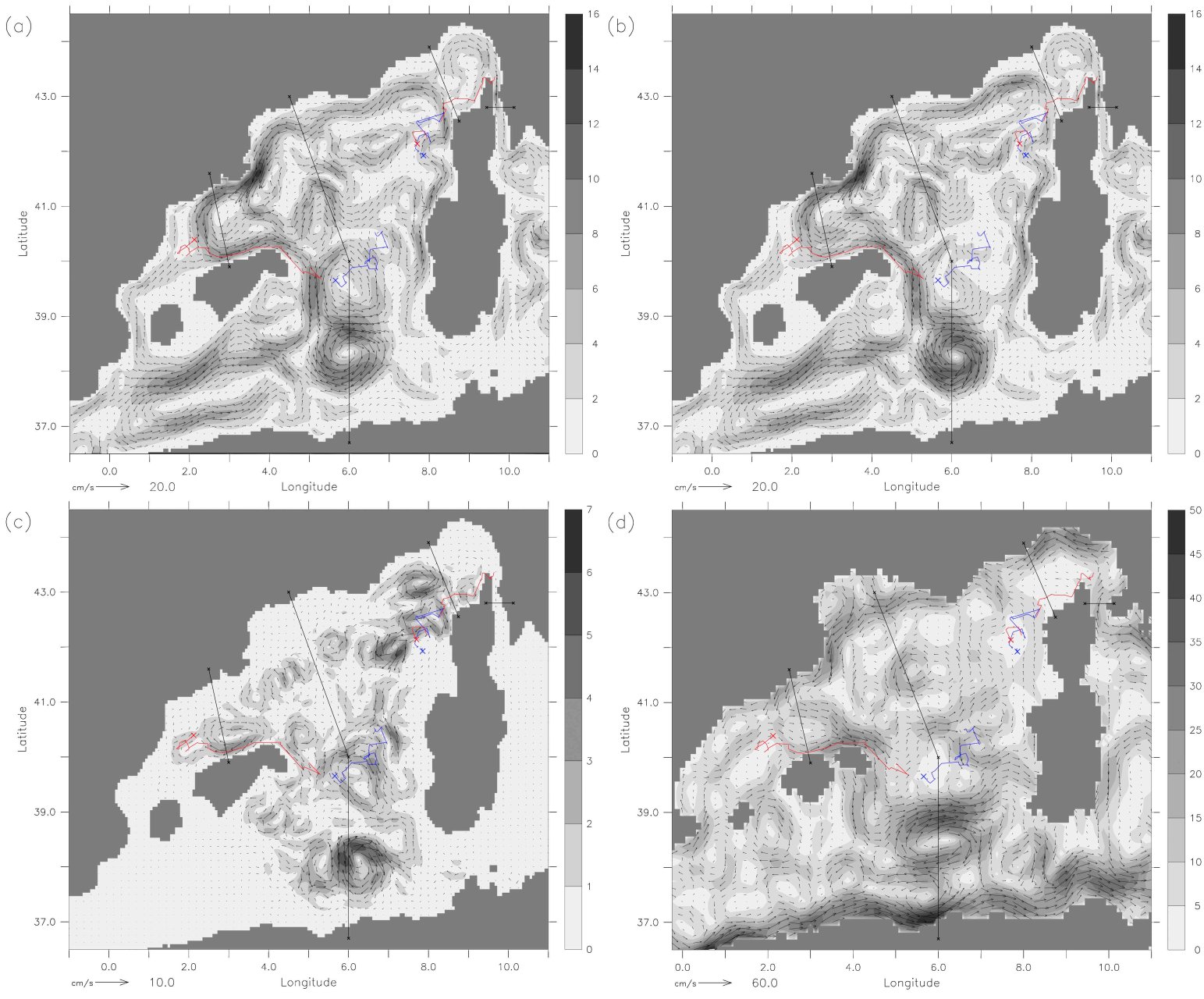
(a)
(b)
(c)
(d)
Latitude
Longitude
43.0
41.0
39.0
37.0
0.0
2.0
4.0
6.0
8.0
10.0
cm/s
20.0
10.0
60.0
0
2
4
6
8
10
12
14
16
1
3
5
7
15
20
25
30
35
40
45
50

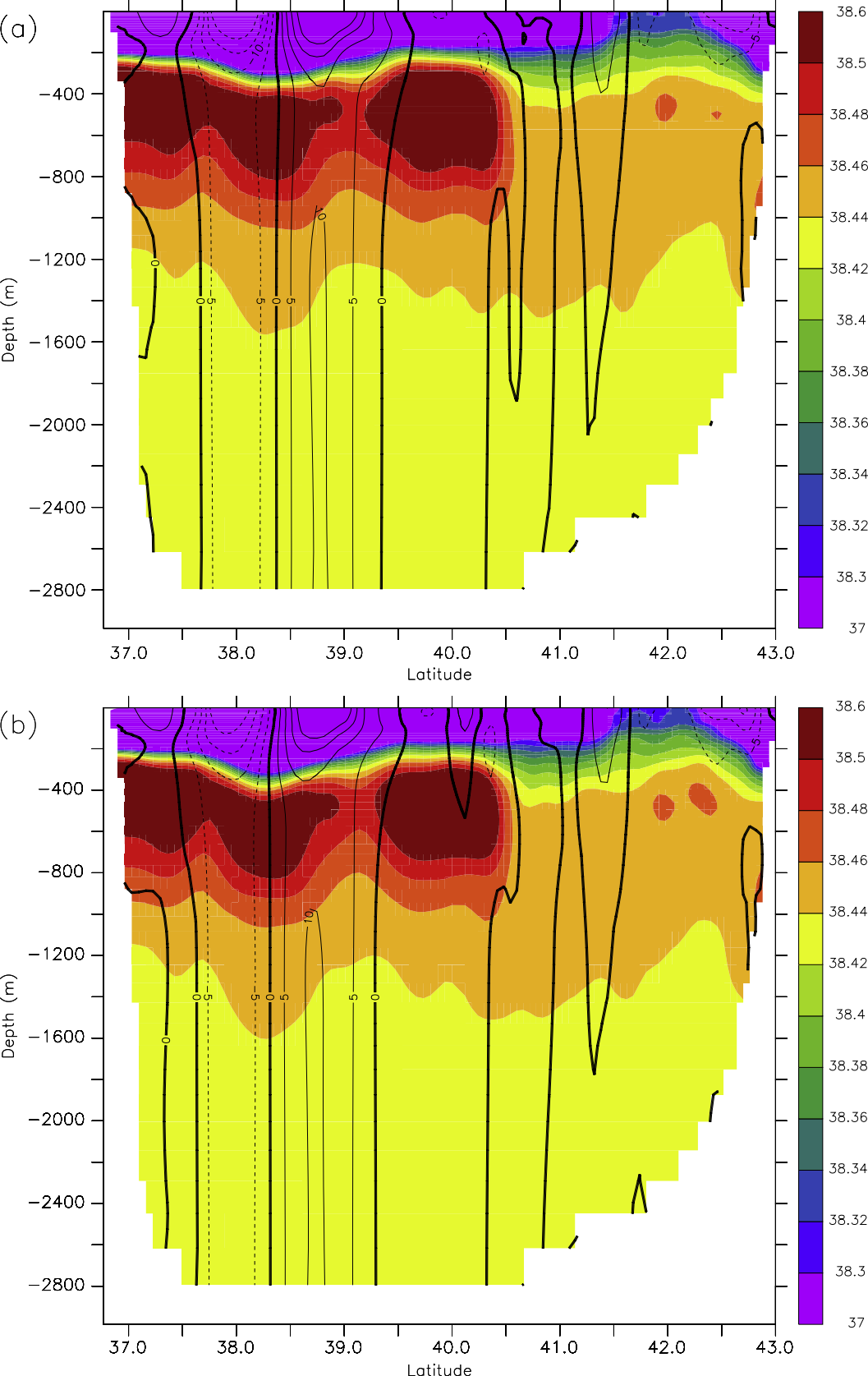
(a)
(b)
Depth (m)
−400
−800
−1200
−1600
−2000
−2400
−2800
37.0
38.0
39.0
40.0
41.0
42.0
43.0
Latitude
38.6
38.5
38.48
38.46
38.44
38.42
38.4
38.38
38.36
38.34
38.32
38.3
37

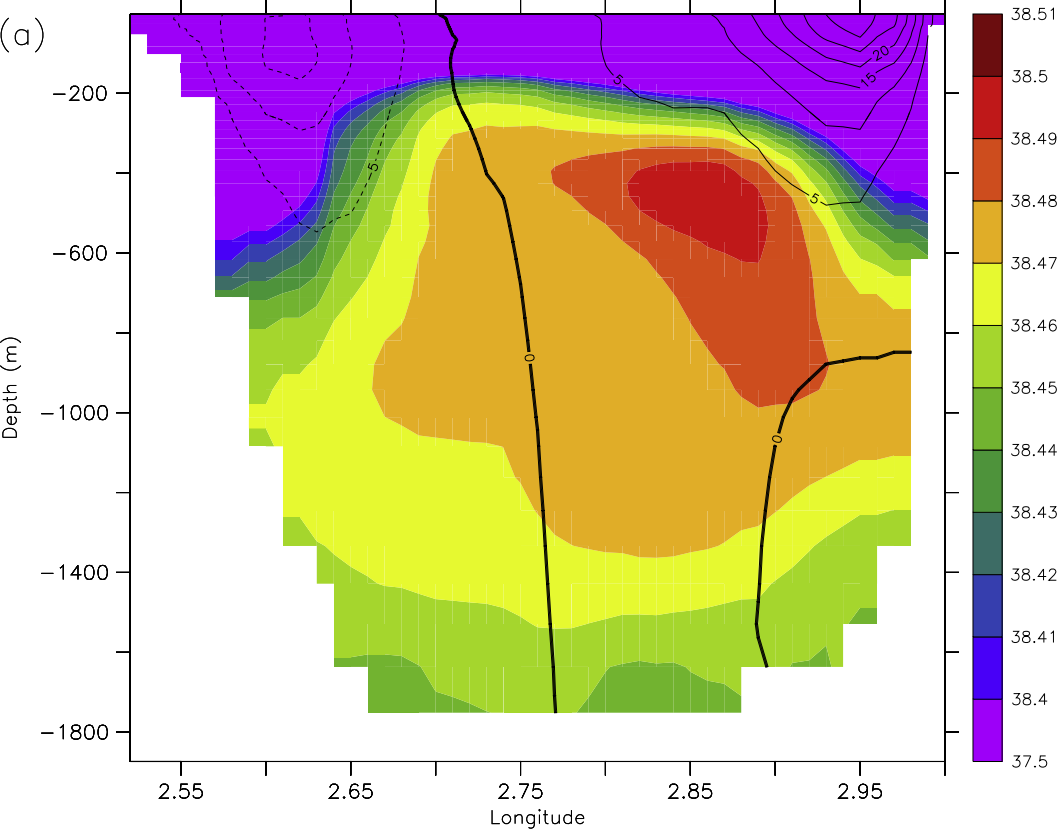
(a)
−200
−600
−1000
−1400
−1800
Depth (m)
2.55
2.65
2.75
2.85
2.95
Longitude
38.51
38.5
38.49
38.48
38.47
38.46
38.45
38.44
38.43
38.42
38.41
38.4
37.5

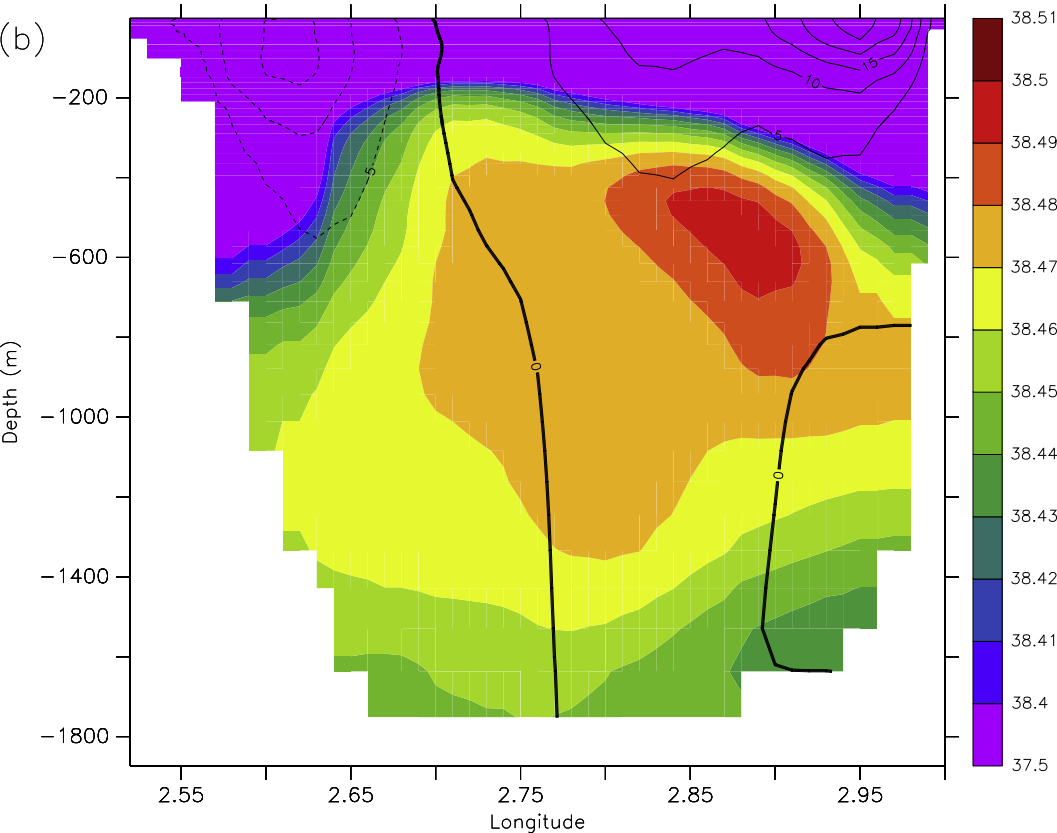
(b)
−200
−600
−1000
−1400
−1800
Depth (m)
2.55
2.65
2.75
2.85
2.95
Longitude
38.51
38.5
38.49
38.48
38.47
38.46
38.45
38.44
38.43
38.42
38.41
38.4
37.5

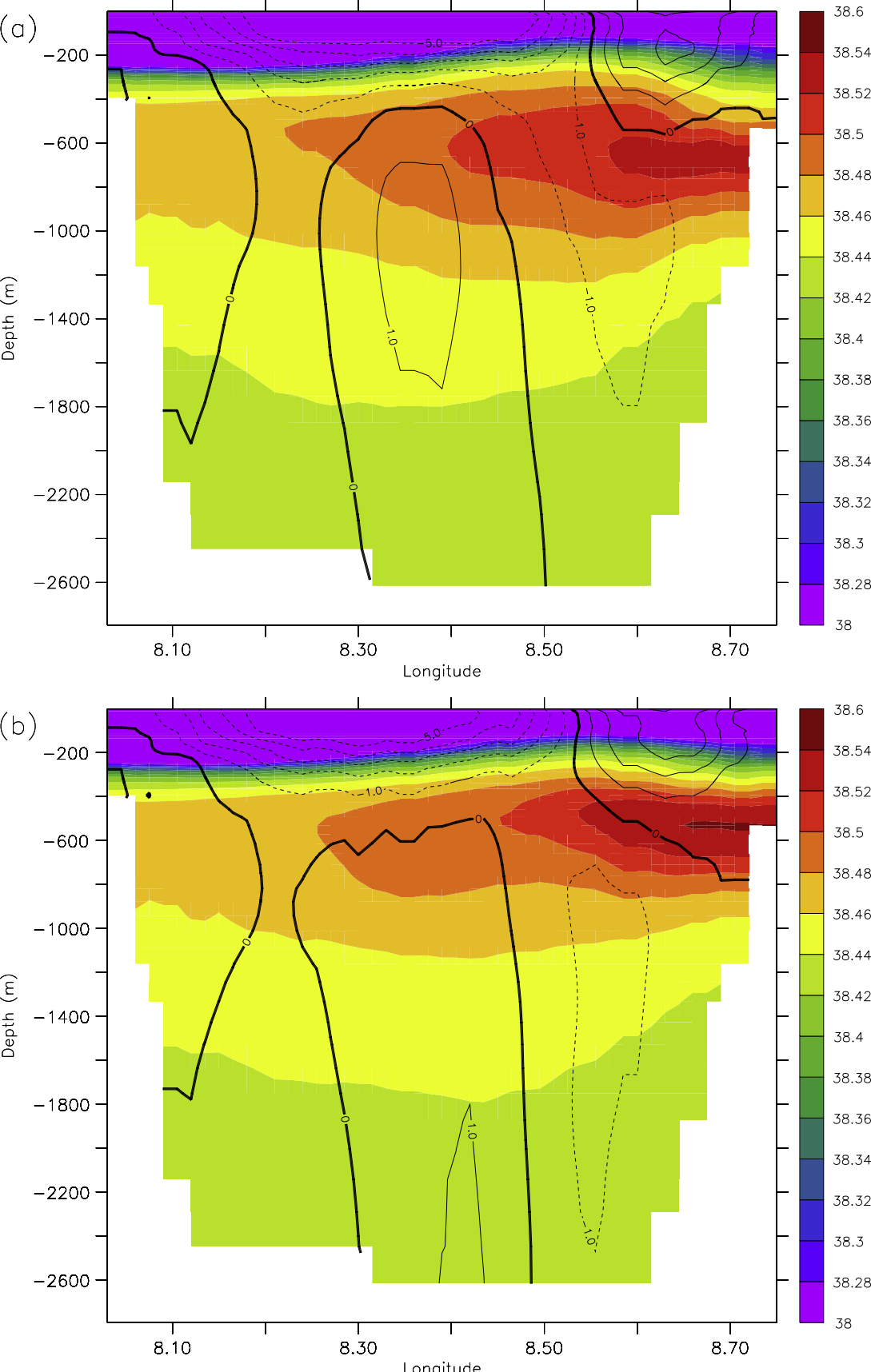
(a)
(b)
Depth (m)
−200
−600
−1000
−1400
−1800
−2200
−2600
8.10
8.30
8.50
8.70
Longitude
38.6
38.54
38.52
38.5
38.48
38.46
38.44
38.42
38.4
38.38
38.36
38.34
38.32
38.3
38.28
38
5.0
1.0
0

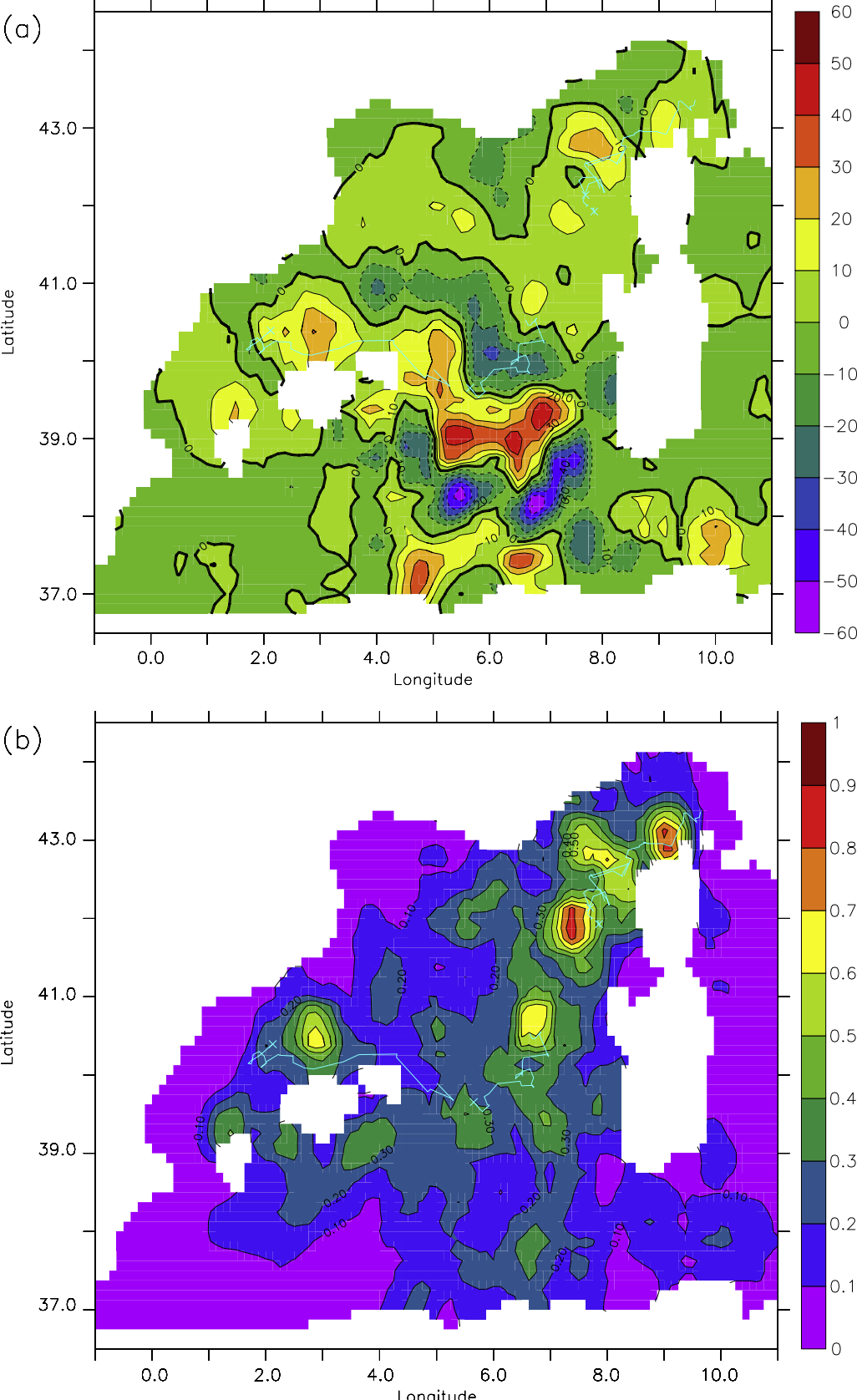
(a)
43.0
41.0
39.0
37.0
Latitude
0.0
2.0
4.0
6.0
8.0
10.0
Longitude
60
50
40
30
20
10
0
−10
−20
−30
−40
−50
−60
(b)
43.0
41.0
39.0
37.0
Latitude
0.0
2.0
4.0
6.0
8.0
10.0
Longitude
1
0.9
0.8
0.7
0.6
0.5
0.4
0.3
0.2
0.1
0

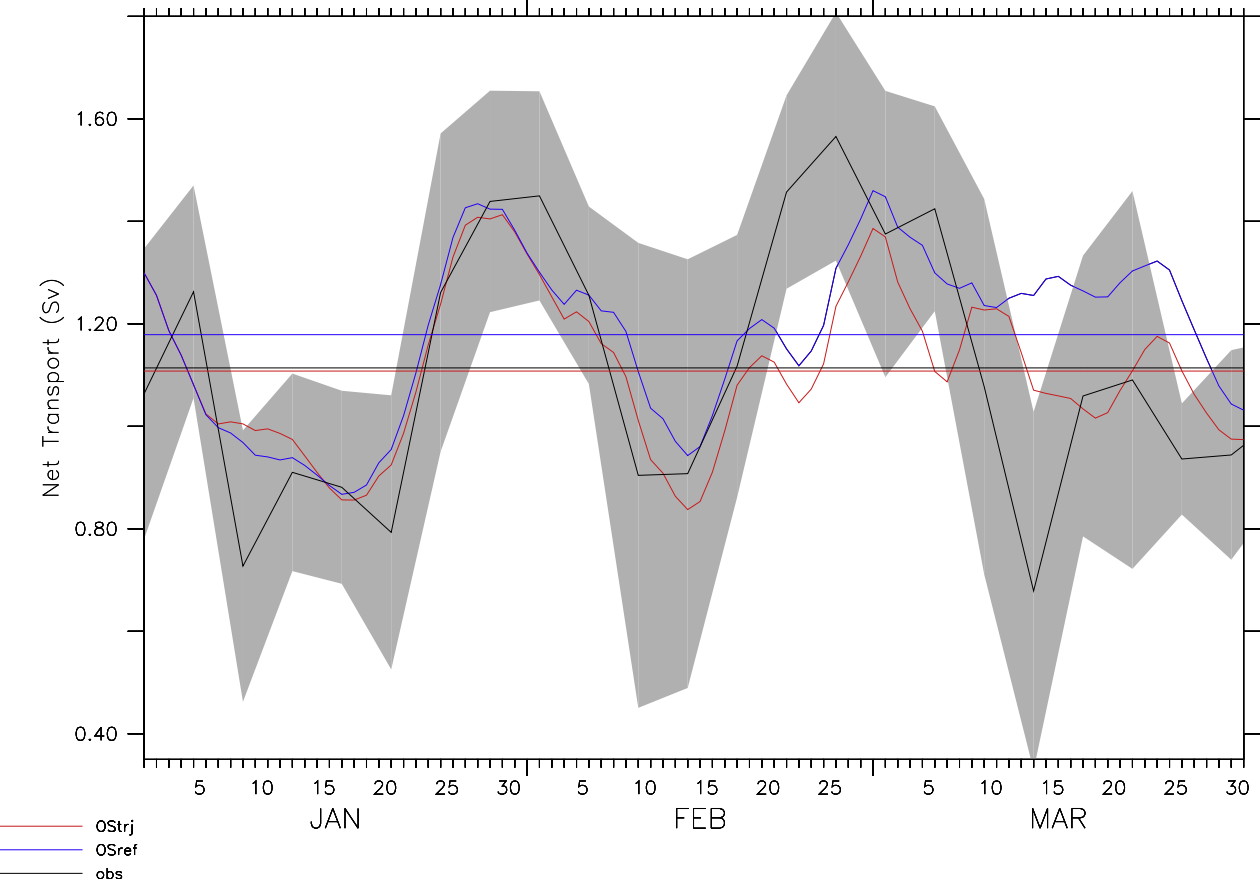
1.60
1.20
0.80
0.40
Net Transport (Sv)
5
10
15
20
25
30
JAN
FEB
MAR
OStrj
OSref
obs